Pflugers Arch - Eur J Physiol (2012) 463:625–633
DOI 10.1007/s00424-012-1082-2

SIGNALING AND CELL PHYSIOLOGY

Regulatory mechanisms underlying the modulation of GIRK1/GIRK4 heteromeric channels by P2Y receptors

Jie Wu · Wei-Guang Ding · Hiroshi Matsuura · Minoru Horie

Received: 17 October 2011 / Revised: 5 February 2012 / Accepted: 6 February 2012 / Published online: 24 February 2012

Abstract The muscarinic K^+ channel ($I_{K,ACh}$) is a hetero-tetramer composed of GIRK1 (Kir3.1) and GIRK4 (Kir3.4) subunits of a G protein-coupled inwardly rectifying channel, and plays an important role in mediating electrical responses to the vagal stimulation in the heart. $I_{K,ACh}$ displays biphasic changes (activation followed by inhibition) through the stimulation of the purinergic P2Y receptors, but the regulatory mechanism involved in these modulation of $I_{K,ACh}$ by P2Y receptors remains to be fully elucidated. Various P2Y receptor subtypes and GIRK1/GIRK4 (I_{GIRK}) were co-expressed in Chinese hamster ovary cells, and the effect of stimulation of P2Y receptor subtypes on I_{GIRK} were examined using the whole-cell patch-clamp method. Extracellular application of 10 μM ATP induced a transient activation of I_{GIRK} through the $P2Y_1$ receptor, which was completely abolished by pretreatment with pertussis toxin. ATP initially caused an additive transient increase in ACh-activated I_{GIRK} (via M_2 receptor), which was followed by subsequent inhibition. This inhibition of I_{GIRK} by ATP was attenuated by co-expression of regulator of G-protein signaling 2, or phosphatidylinositol-4-phosphate-5-kinase, or intracellular phosphatidylinositol 4,5-bisphosphate loading, but not by the exposure to protein kinase C inhibitors. $P2Y_4$ stimulation also persistently suppressed the ACh-activated I_{GIRK}. In addition, I_{GIRK} evoked by the stimulation of the $P2Y_4$ receptor exhibited a transient activation, but that evoked by the stimulation of $P2Y_2$ or $P2Y_{12}$ receptor showed a rather persistent activation. These results reveal (1) that $P2Y_1$ and $P2Y_4$ are primarily coupled to the G_q-phospholipase C-pathway, while being weakly linked to $G_{i/o}$, and (2) that $P2Y_2$ and $P2Y_{12}$ involve $G_{i/o}$ activation.

Keywords GIRK1/GIRK4 · P2Y receptors · I_{GIRK} · PIP_2 · Patch clamp · CHO

Abbreviations

ACh	Acetylcholine
$I_{K,ACh}$	Muscarinic K^+ channel
PLC	Phospholipase C
PKC	Protein kinase C
PIP_2	Phosphatidylinositol 4,5-bisphosphate
PTX	Pertussis toxin
PI4P-5K	Phosphatidylinositol-4-phosphate-5-kinase
CHO	Chinese hamster ovary
AC	Adenylyl cyclase
WT	Wild type
GFP	Green fluorescent protein
ATP	Adenosine triphosphate
UTP	Uridine triphosphate
RGS_2	Regulator of G-protein signaling 2
GIRK	G protein-activated inward rectifier K^+ channel

Jie Wu and Wei-Guang Ding have contributed equally to this work.

Electronic supplementary material The online version of this article (doi:10.1007/s00424-012-1082-2) contains supplementary material, which is available to authorized users.

J. Wu
Department of Pharmacology,
Medical School of Xi'an Jiaotong University,
Xi'an, Shaanxi 710061, People's Republic of China

J. Wu · W.-G. Ding · H. Matsuura (✉)
Department of Physiology, Shiga University of Medical Science,
Otsu, Shiga 520-2192, Japan
e-mail: matuurah@belle.shiga-med.ac.jp

J. Wu · M. Horie (✉)
Department of Cardiovascular and Respiratory Medicine,
Shiga University of Medical Science,
Otsu, Shiga 520-2192, Japan
e-mail: horie@belle.shiga-med.ac.jp

Introduction

The muscarinic K^+ channel ($I_{K,ACh}$) is a heterotetramer that comprises Kir3.1 and Kir3.4 subunits (encoded by GIRK1 and GIRK4, respectively) of G protein-coupled inwardly rectifying channel. $I_{K,ACh}$ plays an important role in mediating negative inotropic, chronotropic, and dromotropic responses to the vagal neurotransmitter acetylcholine (ACh) in the heart [20]. Previous reports indicate that adenosine 5′-triphosphate (ATP) produces dual effects on $I_{K,ACh}$: a transient activation followed by a persistent inhibition, in guinea pig atrial cells [13, 24, 44]. Like other neurotransmitters such as ACh [34, 35] and adenosine [21, 24], ATP activates the membrane receptors coupled to the $I_{K,ACh}$ channel proteins through a pertussis toxin (PTX) sensitive heterotetrameric G protein, thus leading to the dissociation of the heterotrimeric G-protein complex into its α and $\beta\gamma$ subunits that can interact with the channel and cause an increase in open-state probability of the channel [5, 24, 42]. Conversely, $I_{K,ACh}$ is persistently inhibited by ATP following the transient activation. Previous studies using guinea pig atrial cells [25, 44] demonstrated that the inhibition of $I_{K,ACh}$ by ATP is associated with activation of the P2Y receptors that are coupled to a PTX-insensitive G protein leading to activation of G_q-phospholipase C (PLC) signaling pathway. However, the modulatory mechanism underlying the inhibition of $I_{K,ACh}$ by P2Y receptor subtype stimulation has yet to be fully elucidated.

P2Y receptors belong to G protein-coupled P2 purinergic receptors that can be activated by purine or pyrimidine nucleotides. Eight P2Y receptor subtypes ($P2Y_{1, 2, 4, 6, 11, 12, 13}$ and $_{14}$) have been cloned from mammalian cells, and all of them are expressed in heart tissues and associated with the extracellular signaling pathway [3, 10, 30, 37]. Several studies have so far indicated that ATP elicits diverse functional responses in various types of tissues including cardiac cells [10, 26, 27]. However, the functional coupling correlates of the involved P2Y receptor subtypes in cardiac cells is still a topic of debate and remains difficult in native cell due to the restricted availability of subtype-selective ligands and/or blockers.

The present study was undertaken to further explore the inhibitory mechanism of $I_{K,ACh}$ using Chinese hamster ovary (CHO) cells heterologously co-expressed with GIRK1/GIRK4 and different P2Y receptor subtypes. The result reveals that stimulation of $P2Y_1$ or $P2Y_4$ receptor subtype markedly inhibited ACh-activated I_{GIRK} currents by G_q-PLC pathway signaling, although the two receptors were also weakly coupled to $G_{i/o}$ protein to transiently activate I_{GIRK}. On the contrary, $P2Y_2$ and $P2Y_{12}$ receptor subtypes were coupled with $G_{i/o}$ protein to persistently activate I_{GIRK}.

Materials and methods

Heterologous expression of cDNA in CHO cells

Full-length cDNA encoding rat GIRK1 subcloned into the pCI expression vector was a kind gift from Dr. LY Jan (Department of Physiology and Biochemistry, Howard Hughes Medical Institute, University of California). Full-length cDNA encoding rat GIRK4 subcloned into the pCDNA3 expression vector was kindly provided by Dr. JP Adelman (Department of Molecular and Medical Genetics, Oregon Health and Sciences University). Full-length cDNA encoding rat type I phosphatidylinositol-4-phosphate-5-kinase (PI4P-5K) subcloned into pCDNA3 expression vector was generously donated by Dr. Y Oka (Third Department of Internal Medicine, Yamaguchi University School of Medicine, Japan). Full-length cDNA encoding human M_2, α_1, $P2Y_1$, $P2Y_2$, $P2Y_4$, $P2Y_{12}$ receptors and regulator of G protein signaling 2 (RGS_2) subcloned individually into $pCDNA3.1^+$ were all obtained from the University of Missouri–Rolla cDNA Resource Center (Rolla, MO). The experimental cDNAs were transiently transfected into CHO cells together with green fluorescent protein (GFP) cDNA [0.5 μg GFP +1 μg GIRK1+1 μg GIRK4+1 μg P2Ys (or α_1)+1 μg M_2] by using Lipofectamine (Invitrogen Life Technologies, Inc. Carlsbad, CA, USA) according to the manufacturer's instructions. Two micrograms of PI4P-5K or RGS_2 cDNA was co-transfected in subset experiments. The transfected cells were cultured in DMEM/Ham's F-12 medium (Nakalai Tesque Inc., Kyoto, Japan) supplemented with 10% fetal bovine serum (GIBCO) and antibiotics (100 U/ml penicillin and 100 μg/ml streptomycin) in a humidified incubator with 5% CO_2 and 95% air at 37°C. The cultures were passaged every 4 to 5 days using a brief trypsin–EDTA treatment. The trypsin-EDTA treated cells were seeded onto glass coverslips in a petri dish for later patch-clamp experiments.

Solutions and chemicals

The pipette solution contained (mM) 70 potassium aspartate, 40 KCl, 10 KH_2PO_4, 1 $MgSO_4$, 3 Na_2-ATP (Sigma), 0.1 Li_2-GTP (Roche Diagnostics GmbH, Mannheim, Germany), 5 EGTA, and 5 Hepes, and pH was adjusted to 7.2 with KOH. The extracellular solution contained (mM) 140 NaCl, 5.4 KCl, 1.8 $CaCl_2$, 0.5 $MgCl_2$, 0.33 NaH_2PO_4, 5.5 glucose, and 5.0 Hepes, and pH was adjusted to 7.4 with NaOH. Agents added to the extracellular solutions included ACh (Sigma Chemical Co., St. Louis, MO, USA), ATP (Sigma), uridine triphosphate (UTP, Sigma), bisindolylmaleimide 1 (BIS-1, Sigma), chelerychrine (CHE, Sigma), and phenylephrine (PHE, Sigma). ACh, ATP, UTP, and PHE were dissolved in the distilled water to yield 10 mM or 30

mM stock solutions. BIS-1 and CHE were dissolved in dimethyl sulfoxide (DMSO, Sigma) to yield stock solutions of 200 μM and 5 mM, respectively. Phosphatidylinositol 4,5-bisphosphate (PIP_2; Calbiochem, San Diego, CA, USA) was directly dissolved in the control pipette solution at a concentration of 50 μM with 30 min sonication on ice. In a subset of experiments, the cells were pre-incubated with 5 μg/ml PTX (Seikagaku, Japan) for at least 2 h to inhibit a PTX-sensitive G protein, as previously described [16].

Electrophysiological recordings and data analysis

The cells attached to glass coverslips were transferred to a 0.5-ml recording chamber perfused with extracellular solution at 1–2 ml/min after 48 h of transfection. The chamber was mounted on the stage of an inverted microscope (ECLIPSE TE2000-U; Nikon, Tokyo, Japan) and maintained at 25°C. Patch-clamp experiments were conducted on GFP-positive cells. Whole-cell membrane currents were recorded with an EPC-8 patch-clamp amplifier (HEKA, Lambrecht, Germany), and data were low-pass filtered at 1 kHz, acquired at 5 kHz through an LIH-1600 analog-to-digital converter (HEKA) and stored on a hard disc drive, using the PulseFit software program (HEKA). Patch pipettes were fabricated from borosilicate glass capillaries (Narishige, Japan) using a horizontal microelectrode puller (P-97; Sutter Instrument Co., USA), and the tips were then fire-polished using a microforge. Patch pipettes had a resistance of 2.5–4.0 MΩ when filled with the pipette solution. Membrane currents were measured at a holding potential of −40 mV or during the voltage ramp protocol (dV/dt=±0.4 V/s), which consisted of an ascending (depolarizing) phase from the holding potential to +50 mV followed by a descending (hyperpolarizing) phase to −130 mV. The current–voltage (I–V) relationship was determined during descending phase.

All of the averaged data are expressed as the mean ± SEM, with the number of experiments shown in parentheses. Statistical comparisons were analyzed using either Student's unpaired t test or ANOVA followed by Dunnett's *post hoc*, as appropriate. Differences were considered to be statistically significant if a value of $P<0.05$ was obtained.

Results

The nature of I_{GIRK} during exposure to ATP in CHO cells expressing $P2Y_1$ receptor

The effect of extracellular ATP on I_{GIRK} was examined in cells transfected with $P2Y_1$ receptor by measuring whole-cell membrane currents at a holding potential of −40 mV and during hyperpolarizing voltage ramps from +50 to −130 mV. The bath application of 10 μM ATP initially evoked a rapid outward shift of the holding current (I_{GIRK} activation), which then progressively declined to the baseline level within ~1–2 min (a subsequent inward shift, Fig. 1a) despite the continued presence of the agonist.

Figure 1b illustrates the membrane currents during hyperpolarizing voltage ramps, recorded before and during application of ATP. The membrane current was calculated by digital subtraction of the current traces under control conditions from that shortly after ATP application and showed an inward rectification (Fig. 1c). $I_{K,ACh}$ is activated by a membrane-delimited pathway involving a PTX-sensitive G protein ($G_{i/o}$) in guinea-pig atrial myocytes [24]. The present experiment also found that pre-exposure to 5 μg/ml PTX for 2 h abolished the action of extracellular ATP (Fig. 1d), suggesting that a PTX-sensitive G protein mediates the activation of I_{GIRK} by $P2Y_1$ receptor stimulation.

The functional regulation of $P2Y_1$ receptor was further analyzed using 10 μM ACh to induce an activation of I_{GIRK} at −40 mV (Fig. 2a). The further addition of ATP initially had an additive effect on ACh-activated I_{GIRK} but then markedly inhibited the current (Fig. 2a; the number of cells

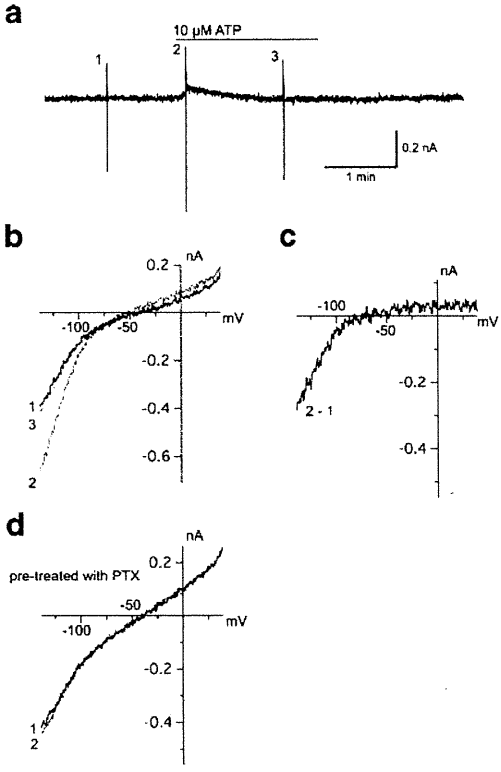

Fig. 1 Effect of ATP on the activation of I_{GIRK} in CHO cells transfected with $P2Y_1$ receptor. **a** The whole-cell currents recorded at a holding potential of −40 mV and during exposure to 10 μM ATP. **b** Superimposed I–V relationships measured during the voltage ramps applied at the points indicated by numbers (*1–3*) in panel (**a**). **c** I–V relationship obtained by digital subtraction of current traces as indicated. **d** After pretreatment with 5 μg/ml PTX for 2 h, the I–V relationships were measured during the voltage ramps

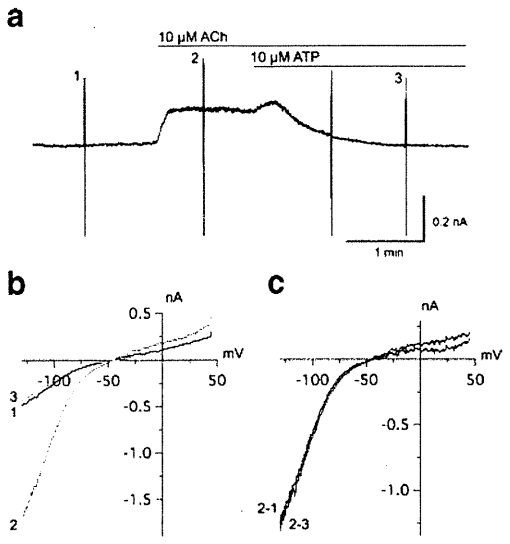

Fig. 2 Inhibition of ACh-activated I_{GIRK} by ATP. **a** The whole-cell currents recorded at a holding potential of −40 mV and during voltage ramps applied before (*1*), during exposure to 10 μM ACh (*2*), and after further addition of 10 μM ATP (*3*). **b** Superimposed *I–V* relationships measured during the voltage ramps applied at the points indicated by numerals (*1–3*) in panel (**a**). **c** Superimposed *I–V* relationships for the difference currents obtained by digital subtraction of current records as indicated. The voltage ramp traces were truncated for the purpose of presentation

positively responded to ATP was 18/19). The ACh-activated maximal I_{GIRK} was decreased by 92.44±10.61% (n=19), when measured 3 min after application of 10 μM ATP, which indicates that external ATP almost inhibited the ACh-activated I_{GIRK}. Figure 2b and c show that the ACh-activated I_{GIRK} current also exhibited an inwardly rectifying *I–V* relationship, which is consistent with the properties of $I_{K.ACh}$ in guinea-pig atrial myocytes. In addition, I_{GIRK} isolated by digital subtraction of the currents in the presence of ACh from that after ATP application also exhibited an inwardly rectifying *I–V* relationship.

In different sets of experiments, we examined the background currents and the expression ability of our CHO cell expression system. The results show that bath application of ACh and ATP could not induce any discernible currents in non-transfected cells (Fig. S1a) and in cells transfected only with GFP + GIRK1/GIRK4 (Fig. S1b). However, ACh evoked persistent I_{GIRK} currents in cells transfected with GFP + GIRK1/GIRK4 + M_2 (Fig. S1c), which was consistently inhibited by ATP when co-transfected with $P2Y_1$ in addition to GIRK subunits and M_2 (Fig. S1d). Figure S1e shows the representative image of the cells showing GFP expression. On the other hand, the inhibition of I_{GIRK} currents was not observed in cells without $P2Y_1$ transfection (Fig. S1c). These results indicate that functional expression of intrinsic P2Y and M_2 receptors was almost null in our CHO cell expression system, and all plasmids were successfully expressed in our cells. To exclude the possibility that the activation of I_{GIRK} was affected by G protein-coupled receptor–G protein interaction, we observed the effects of ATP on ACh-activated I_{GIRK} in CHO cells co-transfected lower doses (0.2–0.5 μg) of $P2Y_1$ together with 0.5 μg GFP +1 μg GIRK1/GIRK4+1 μg M_2. Figure S1f shows that the inhibition of ACh-activated I_{GIRK} by ATP in cells co-transfected with 0.2 μg $P2Y_1$ is almost the same as that co-transfected with 1 μg $P2Y_1$.

The modulation of RGS_2 on ATP-induced inhibition of I_{GIRK}

Regulators of G-protein signaling (RGS) proteins modulate the signal transduction via G protein-coupled receptors (GPCR). These proteins enhance GTP hydrolysis by accelerating the intrinsic GTPase activity of Gα-subunit, and thereby terminate the G protein activation cycle [4, 31, 39]. RGS_2 (one of the important inhibitor of $G_q\alpha$ subunit) was co-transfected with GIRK1/GIRK4, M_2 and $P2Y_1$ cDNAs to explore the inhibitory mechanism of ATP on I_{GIRK}. Figure 3a shows that the inhibitory action of ATP on ACh-activated I_{GIRK} was significantly attenuated with the co-expression of RGS_2. Figure 3c shows that the inhibitory degree of the ACh-activated I_{GIRK} was only 50.7± 9.1% (n=15) 3 min after exposure to 10 μM ATP, which

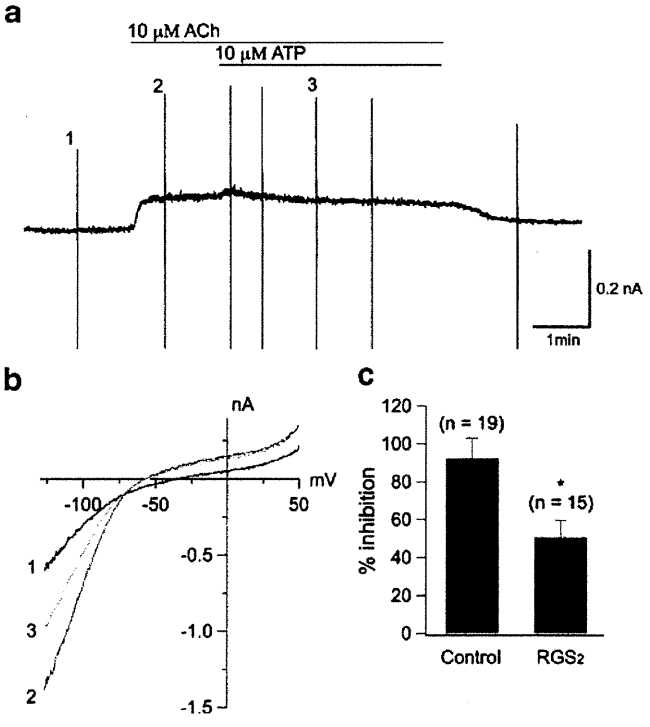

Fig. 3 The modulation of RGS_2 on the ATP-induced inhibition of I_{GIRK}. **a** Whole-cell currents recorded in CHO cell co-transfected with RGS_2 at a holding potential of −40 mV. **b** Superimposed *I–V* relationships measured during the voltage ramps applied at the points indicated by numerals (*1–3*) in panel (**a**). **c** ATP-induced inhibition of I_{GIRK} (*P<0.05 vs. control)

is significantly ($P<0.05$) lower than that of control (92.44± 10.61%, $n=19$). Therefore, the activation of G_q protein is involved in the ATP-induced inhibition of I_{GIRK}. Besides, our supplementary experiment data observed in CHO cells co-transfected 1 μg M_1 receptor (coupled with G_q) together with 0.5 μg GFP+1 μg GIRK1+1 μg GIRK4+1 μg M_2 (Fig. S3a) also supports the result that the activation of G_q protein is involved in the agonist-induced inhibition of I_{GIRK} in this experiment.

In order to further confirm the result that co-expression of RGS_2 led to the inhibition of the signal transduction via G_q protein-coupled receptors in our cell expression system, we co-transfected GFP + GIRK1/GIRK4+M_2+RGS_2 together with α_1-adrenergic receptor that has been generally accepted to be coupled to G_q [8]. Similar to the inhibition of ACh-activated I_{GIRK} currents by ATP, bath application of PHE (a selective α_1 receptor agonist, 30 μM) significantly inhibited the ACh-activated I_{GIRK} currents by 94.8±10.1% ($n=7$) in cells co-expressing α_1 receptor (Fig. S2a), whereas only by 40.3±5.4% ($n=5$, $P<0.01$) in cells co-expressing $RGS_2+\alpha_1$ receptor (Fig. S2b), implicating that the attenuation of I_{GIRK} inhibition by ATP in cells co-expressing RGS_2 is involved in blockade of G_q protein in our experiment.

Role of membrane PIP_2 in ATP-induced decline of I_{GIRK}

A previous study indicated that ATP receptor stimulation could inhibit the $I_{K,ACh}$ channels through depletion of membrane PIP_2 in guinea pig atrium [44]. PI4P-5K (the enzyme that catalyzes PIP_2 synthesis [11]) was co-expressed with GIRK1/GIRK4, M_2, and $P2Y_1$ cDNAs. Figure 4a shows that the co-expression of PI4P-5K markedly ($P<0.01$) prevented the inhibitory action of ATP on ACh-activated I_{GIRK}, compared with that in control (55.2±10.0%, $n=13$ vs. 92.44 ±10.61%, $n=19$; Fig. 4c). This result is consistent with the view that a characteristic progressive decline of I_{GIRK} in the presence of extracellular ATP is mediated through the depletion of membrane PIP_2.

If the reduction in membrane PIP_2 underlies the decline of I_{GIRK} during exposure to ATP, intracellular loading of exogenous PIP_2 may attenuate the inhibitory action of ATP on ACh-activated I_{GIRK}. As demonstrated in Fig. 5a and b, intracellular dialysis of 50 μM PIP_2 for 5–7 min through a recording pipette significantly reduced the inhibition degree of ACh-activated I_{GIRK} by ATP. The inhibition of I_{GIRK} (Fig. 5c) only reached 18.2±6.4% ($n=5$) 3 min after bath application of 10 μM ATP, which is markedly ($P<0.01$) lower than that of the control (92.44±10.61%, $n=19$). This result further indicates that the reduction in membrane PIP_2 is closely linked to the inhibitory action of ATP on I_{GIRK}.

PKC activation was previously reported to produce inhibitory action on $I_{K,ACh}$ [14, 22, 31, 35]. In our experiments, however, bath application of two different PKC

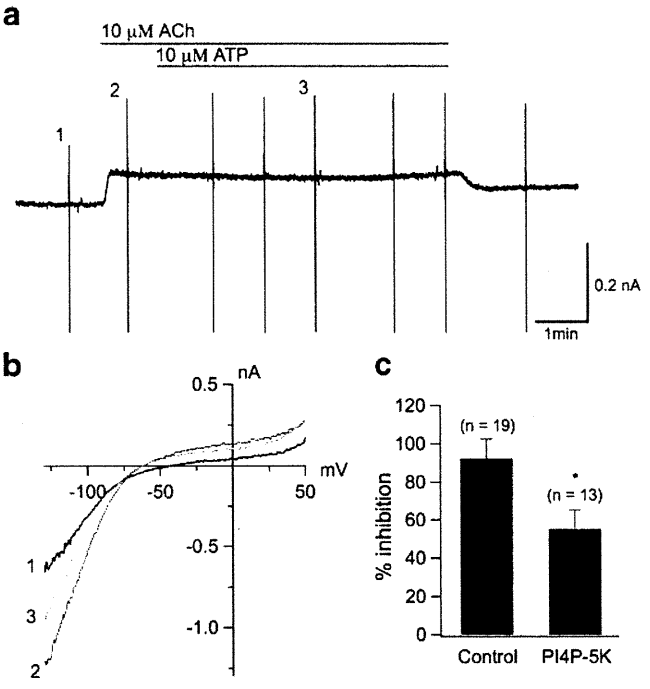

Fig. 4 Co-expression of PI4P-5K attenuated the ATP-induced inhibition of I_{GIRK}. **a** The whole-cell currents recorded in CHO cell co-transfected with PI4P-5K in the presence of ACh and ATP at a holding potential of −40 mV. **b** Superimposed *I–V* relationships measured during the voltage ramps applied at the points indicated by numerals (*1–3*) in panel (**a**). **c** ATP-induced inhibition of I_{GIRK} (*$P<0.05$ vs. control)

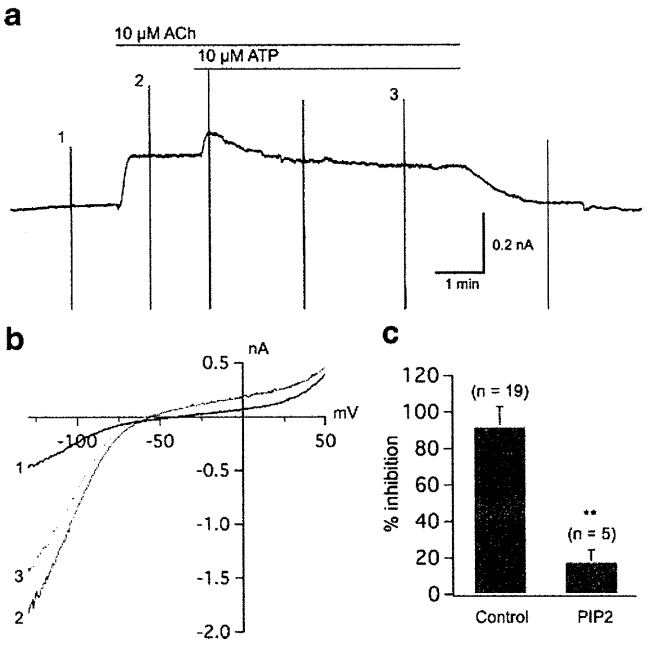

Fig. 5 Effect of PIP_2 (intracellularly loaded) on the ATP-induced inhibition of I_{GIRK}. **a** Whole-cell currents recorded with PIP_2 intracellular dialysis for 5–7 min at a holding potential of −40 mV, and then in the presence of ACh and ATP. **b** Superimposed *I–V* relationships measured during the voltage ramps applied at the points indicated by numerals (*1–3*) in panel (**a**). **c** ATP-induced inhibition of I_{GIRK} (**$P<0.01$ vs. control)

inhibitors, bisindolylmaleimide (BIS-1, 200 nM, Fig. 6a and b) and chelerythrine (CHE, 5 μM, Fig. 6b), did not significantly alter the inhibition degree of ACh-activated I_{GIRK} by ATP (control, 92.44±10.61%, n=19; BIS-I, 95.7±15.0%, n=7; CHE, 92.3±17.5%, n=6), thus suggesting that PKC activation is not involved in the ATP-induced inhibition of I_{GIRK} [7, 28].

Effects of P2Y receptor subtype stimulation on I_{GIRK}

Different P2Y receptor subtpes, namely $P2Y_2$, $P2Y_4$, and $P2Y_{12}$, were respectively transfected together with GIRK1/GIRK4 channels to explore the effects of the P2Y receptor stimulation on I_{GIRK}. In the experiment, 10 μM UTP was used as an alternative to ATP to activate $P2Y_2$ and $P2Y_4$ receptors because it seems that these two receptors are more sensitive to UTP [38, 41]. Figure 7a shows the representative I_{GIRK} traces elicited by stimulating $P2Y_2$, $P2Y_4$, and $P2Y_{12}$ receptors, respectively. The persistent I_{GIRK} currents elicited by the stimulation of $P2Y_2$ or $P2Y_{12}$ receptor suggest that little membrane PIP_2 was depleted, whereas the current evoked by the stimulation of $P2Y_4$ receptor was transient, which suggests that depletion of membrane PIP_2 occurred. Figure 7b and c shows the amplitudes of I_{GIRK} normalized to the peak amplitude one minute (I_{1min}/I_{peak}) and 3 min (I_{3min}/I_{peak}) after application of an agonist. The normalized amplitude of I_{GIRK} for $P2Y_2$ or $P2Y_{12}$ was significantly (P<0.01) larger than that of $P2Y_1$ both 1 and 3 min after application of an agonist, whereas the amplitude of I_{GIRK} for $P2Y_1$ or $P2Y_4$ 3 min after receptor stimulation was significantly (P<0.05) lower than that for the same receptor 1 min after receptor stimulation.

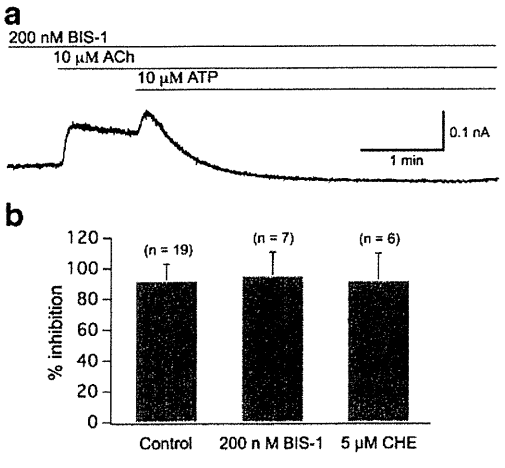

Fig. 6 PKC inhibitors did not attenuate the ATP-induced inhibition of I_{GIRK}. **a** The whole-cell currents recorded in CHO cell pre-treated with 200 nM BIS-1 in the presence of ACh and ATP at a holding potential of −40 mV. **b** ATP-induced inhibition of I_{GIRK} in the presence of 200 nM BIS-1 or 5 μM CHE

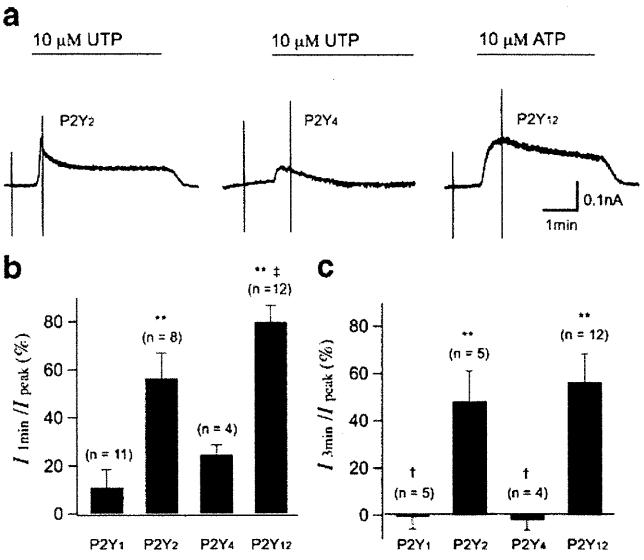

Fig. 7 Comparison of I_{GIRK} currents evoked by stimulating different P2Y receptor subtypes. **a** The whole-cell currents in CHO cells transfected with $P2Y_2$, $P2Y_4$, and $P2Y_{12}$ receptor subtypes at a holding potential of −40 mV. **b** Inhibition of I_{GIRK} 1 min after stimulation of $P2Y_2$, $P2Y_4$, and $P2Y_{12}$ receptors. **c** Inhibition of I_{GIRK} 3 min after stimulation of $P2Y_2$, $P2Y_4$, and $P2Y_{12}$ receptors (**P<0.01 vs. $P2Y_1$ or $P2Y_4$; $^{‡}P$<0.05 vs. $P2Y_2$; ^{+}P<0.05 vs. I_{1min}/I_{peak})

Treatment with 10 μM ACh was first used to induce an I_{GIRK} current at −40 mV, and then 10 μM UTP or ATP was employed to stimulate $P2Y_2$, $P2Y_4$, or $P2Y_{12}$ to further examine the effects of $P2Y_s$ receptor stimulation on ACh-activated I_{GIRK}. Figure 8a and b shows that the nature of the current evoked by stimulating $P2Y_4$ receptor with UTP was almost the same as that elicited by stimulating $P2Y_1$ (Fig. 2). The inhibitory degree of ACh-activated I_{GIRK} by the stimulation of $P2Y_4$ was 99.6±22.5% (n=5), which was similar to that evoked by the stimulation of $P2Y_1$ receptor (Fig. 8c). Figure S3b and c shows that addition of an agonist (ATP or UTP) caused the ACh-activated I_{GIRK} to increase further (there was 1/13 cell co-transfected with $P2Y_2$ that did not respond to UTP). The addition activation of I_{GIRK} by the stimulation of $P2Y_2$ declined slightly, but still much higher than the ACh-activated I_{GIRK} level 3 min after treatment with UTP (Fig. S3b). On the other hand, the addition activation of I_{GIRK} by the stimulation of $P2Y_{12}$ almost did not decline (Fig. S3c).

Discussion

The activation of $I_{K,ACh}$ is due to the activation of $G_{i/o}$ protein [34]. The rapid activation phase of $I_{K,ACh}$ evoked by exposure to ATP is caused by stimulation of P2Y receptor, leading to a membrane-delimited, $G_{i/o}$-mediated channel activation in guinea-pig atrial myocytes [14, 25, 44]. However, there is no consensus on the mechanism of $I_{K,ACh}$

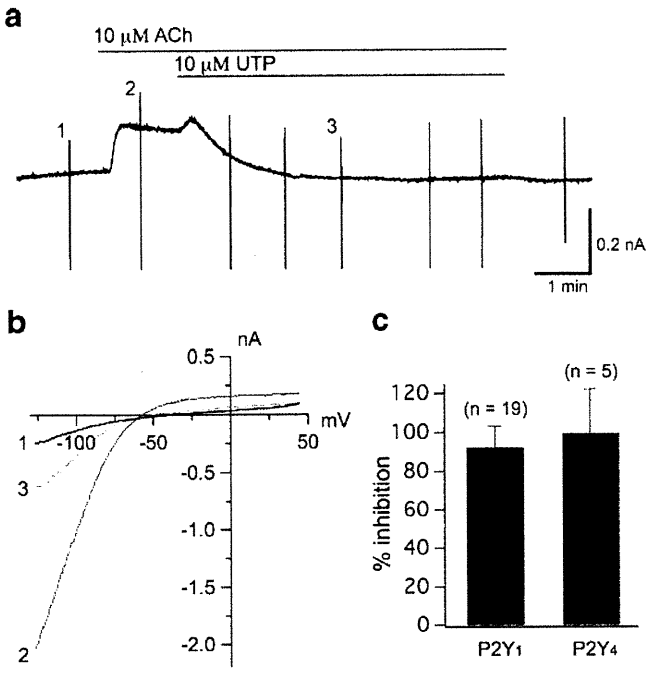

Fig. 8 Effect of $P2Y_4$ stimulation on ACh-activated I_{GIRK}. **a** The whole-cell currents recorded at a holding potential of −40 mV, and in the presence of ACh and UTP. **b** Superimposed *I–V* relationships measured during the voltage ramps applied at the points indicated by numerals (*1–3*) in panel (**a**). **c** Inhibitory degree of I_{GIRK} by the stimulation of $P2Y_1$ and $P2Y_4$ receptors

inhibition produced by agonists. Several groups [7, 14, 18, 25, 29, 44] reported that activation of PLC contributes to the inhibition of $I_{K,ACh}$ by decreasing membrane PIP_2. However, others [15, 23, 32, 36] suggest that the downstream activation of PKC underlies the inhibition of $I_{K,ACh}$. There are also some pieces of evidence to suggest that reduction in membrane PIP_2 and PKC activation are both involved in the $I_{K,ACh}$ inhibition by agonists such as carbachol [22] and ACh [17].

A previous study in the guinea-pig atrium indicated that the inhibition of $I_{K,ACh}$ by extracellular ATP is attenuated by blocking PLC activity with compound 48/80 and by exogenously adding PIP_2 in the atrial myocytes [44]. This observation suggests that the ATP-induced activation of PLC and the concomitant reduction of PIP_2 contribute to the inhibition of $I_{K,ACh}$ by ATP. In addition, RGS_2 protein is one of the important inhibitor of the $G_q\alpha$ subunit and terminates G_q signaling through its GTPase-activating protein mechanism [4, 31, 39]. The present experiment found that co-expression of RGS_2 significantly reduced the ATP-induced inhibition of I_{GIRK}, thus confirming the view that the inhibition of I_{GIRK} by ATP is mediated through the G_q protein-coupled P2Y receptors in native cardiac myocytes [14, 25]. The present study also demonstrated that the ATP-induced inhibition of I_{GIRK} is markedly attenuated by both co-expression of PI4P-5K and intracellular dialysis with PIP_2 in CHO cells. These data are consistent with a previous study in guinea-pig atrial myocytes [44] and support the view that a decrease in membrane PIP_2 is closely linked to the ATP-induced inhibition of $I_{K,ACh}$. In contrast to the study of Keselman et al. [17], however, the PKC inhibitor BIS-1 and CHE did not alter the inhibition of ATP on ACh-activated I_{GIRK}, thus indicating PKC activation might not be involved in the inhibition of I_{GIRK} by ATP [9, 28]. Taken together, the current data fully support the hypothesis that the reduction in membrane PIP_2 via activation of G_q-PLC is mainly responsible for the inhibition of $I_{K,ACh}$ channels by externally applying ATP.

Previous reports have indicated that $P2Y_1$, $P2Y_2$, and $P2Y_4$ receptor subtypes are coupled to PTX-insensitive G_q proteins that activate PLC and then produce a fall in membrane PIP_2 levels, whereas $P2Y_{12}$ receptor is only coupled to PTX-sensitive $G_{i/o}$ protein to inhibition of adenylate cyclase [1, 9, 37, 41]. However, the coupling to signaling transduction pathways appears to be much more complex. An example is that the G_q-coupled $P2Y_1$ receptor, known to inhibit GIRK channels, efficiently activates GIRK1/GIRK2 channels in cultured rat sympathetic neurons [12]. A sequence analysis also indicates that the two regions (the third intracellular loop and the C-terminal tail), implicated in G protein specificity, vary greatly among the P2Y receptor subtypes [40]. The present study found that the stimulation of $P2Y_1$ or $P2Y_4$ receptor evoked a transient activation of I_{GIRK} followed by a persistent inhibition (Figs. 1a and 7a), thus suggesting that a large amount of membrane PIP_2 was consumed via activation of G_q-PLC pathway. This result might implicate that the two receptors are mainly coupled to G_q protein. Contrary to previous reports [1, 9, 37, 41], however, the activation phase of I_{GIRK} evoked by the stimulation of these two receptors reflects the existence of $G_{i/o}$ coupling although it might be relatively weak. In contrast, the stimulation of $P2Y_2$ or $P2Y_{12}$ receptor induced a persistent activation of I_{GIRK} (Fig. 7a), indicating that little membrane PIP_2 was consumed and resultantly implicating that these two receptors are mainly coupled to $G_{i/o}$ protein. Bodor and colleagues have found that purified $P2Y_{12}$ receptor can form a functional receptor when reconstituted with G_i protein, but not when reconstituted with G_q protein [6]. This is consistent with the present finding that the $P2Y_{12}$ receptor is coupled to $G_{i/o}$ protein to activate I_{GIRK}. In addition, the decay I_{GIRK} evoked by the stimulation of $P2Y_2$ was relatively rapid in comparison to the $P2Y_{12}$, suggesting that some amount of membrane PIP_2 was still consumed during the stimulation of $P2Y_2$ and resultantly implicating that $P2Y_2$ is also weakly coupled to G_q protein. The $P2Y_2$ receptor is generally classified to the (PTX-resistant) G_q-coupled subfamily [9, 19, 41]. However, the data in the present study suggested that $P2Y_2$ is also coupled to $G_{i/o}$ protein as suggested by other researchers [37], though they

believed that $P2Y_2$ receptor primarily mediates its function through coupling to G_q. Furthermore, these data are also supported by the fact that $P2Y_2$ receptor is sensitive to PTX in stable expressed astrocytoma cells [33] and in human erythroleukemia cells [2].

There is an abundant expression of $P2Y_2$ mRNA in both human atria and ventricles, whereas the mRNA level of $P2Y_2$ is lower than that of $P2Y_1$ or $P2Y_4$ in mouse cardiomyocytes [43]. Musa and colleagues [30] have also indicated that the $P2Y_2$ mRNA level is the most abundant of the eight P2Y receptors in the human right atrium, but is lower than $P2Y_1$ in human sinoatrial node (SAN). They also found that the distribution of P2Y receptor subtypes in rat right atrium, left ventricle, and SAN is quite different with those in the human heart. These results indicate that the P2Y receptor expression varies greatly in the heart, implicating that responses to the stimulation of P2Y receptor are also diverse in different types of cardiac cells. The current study may contribute to understanding the precise regulatory mechanisms underlying the cardiac signaling pathway mediated by P2Y receptors.

Acknowledgements This study was supported by grants (No. 22590205 and No. 22590206) from the Ministry of Education, Science, and Culture of Japan; the Uehara Memorial Foundation; and health science research grants from the Ministry of Health, Labor and Welfare of Japan for Clinical Research on Measures for Intractable Diseases.

Ethical standards The authors declare that the experiment comply with the current laws of Japan.

Conflict of interest The authors declare that they have no conflict of interest.

References

1. Abbracchio MP, Burnstock G, Boeynaems JM, Barnard EA, Boyer JL, Kennedy C, Knight GE, Fumagalli M, Gachet C, Jacobson KA, Weisman GA (2006) International Union of Pharmacology LVIII: update on the P2Y G protein-coupled nucleotide receptors: from molecular mechanisms and pathophysiology to therapy. Pharmacol Rev 58:281–341
2. Baltensperger K, Porzig H (1997) The P_{2U} purinoceptor obligatorily engages the heterotrimeric G protein G_{16} to mobilize intracellular Ca^{2+} in human erythroleukemia cells. J Biol Chem 272:10151–10159
3. Banfi C, Ferrario S, De Vincenti O, Ceruti S, Fumagalli M, Mazzola A, D'Ambrosi N, Volonte C, Fratto P, Vitali E, Burnstock G, Beltrami E, Parolari A, Polvani G, Biglioli P, Tremoi E, Abbracchio MP (2005) P2 receptors in human heart: upregulation of P2X6 in patients undergoing heart transplantation, interaction with TNFalpha and potential role in myocardial cell death. J Mol Cell Cardiol 39:929–939
4. Bernstein LS, Ramineni S, Hague C, Cladman W, Chidiac P, Levey AL, Hepler JR (2004) RGS2 binds directly and selectively to the M1 muscarinic acetylcholine receptor third intracellular loop to modulate Gq/11alpha signaling. J Biol Chem 279:21248–21256
5. Birnbaumer L (2007) Expansion of signal transduction by G proteins. The second 15 years or so: from 3 to 16 α subunits plus $\beta\gamma$ *dimmers. Biochim Biophys Acta 1768:772–793*
6. Bodor ET, Waldo GL, Hooks SB, Corbitt J, Boyer JL, Harden TK (2003) Purification and functional reconstitution of the human $P2Y_{12}$ receptor. Mol Pharmacol 64:1210–1216
7. Cho H, Lee D, Lee SH, Ho WK (2005) Receptor-induced depletion of phosphatidylinositol 4,5-bisphosphate inhibits inwardly rectifying K^+ channels in a receptor-specific manner. Proc Natl Acad Sci USA 102:4643–4648
8. Docherty JR (2010) Subtypes of functional alpha1-adrenoceptor. Cell Mol Life Sci 67:405–417
9. Erb L, Liao Z, Seye CI, Weisman GA (2006) P2 receptors: intracellular signaling. Pflugers Arch 452:552–562
10. Erlinge D, Burnstock G (2008) P2 receptors in cardiovascular regulation and disease. Purinergic Signalling 4:1–20
11. Falkenburger BH, Jensen JB, Hille B (2010) Kinetics of PIP2 metabolism and KCNQ2/3 channel regulation studied with a voltage-sensitive phosphatase in living cells. J Gen Physiol 135:99–114
12. Filippov AK, Fernandez-Fernandex JM, Marsh SJ, Simon J, Barnard EA, Brown DA (2004) Activation and inhibition of neuronal G protein-gated inwardly rectifying K(+) channels by P2Y nucleotide receptors. Mol Pharmacol 66:468–477
13. Friel DD, Bean BP (1990) Dual control by ATP and acetylcholine of inwardly rectifying K^+ channels in bovine atrial cells. Pflugers Arch 415:651–657
14. Hara Y, Nakaya H (1997) Dual effects of extracellular ATP on the muscarinic acetylcholine receptor-operated K^+ current in guinea-pig atrial cells. Eur J Pharmacol 324:295–303
15. Hill JJ, Peralta EG (2001) Inhibition of a G_i-activated potassium channel (GIRK1/4) by the G_q-coupled m1 muscarinic acetylcholine receptor. J Biol Chem 276:5505–5510
16. Hwang TC, Horie M, Nairn AC, Gadsby DC (1992) Role of GTP-binding proteins in the regulation of mammalian cardiac chloride conductance. J Gen Physiol 99:465–489
17. Keselman I, Fribourg M, Felsenfeld DP, Logothetis DE (2007) Mechanism of PLC-mediated Kir3 current inhibition. Channels (Austin) 1:113–123
18. Kobrinsky E, Mirshahi T, Zhang H, Jin T, Logothetis DE (2000) Receptor-mediated hydrolysis of plasma membrane messenger PIP2 leads to K^+-current desensitization. Nat Cell Biol 2:507–514
19. Koles L, Gerevich Z, Oliveira JF, Zadori ZS, Wirkner K, Illes P (2008) Interaction of P2 purinergic receptors with cellular macromolecules. Naunyn-Schmiedeberg's Arch Pharmacol 377:1–33
20. Krapivinsky G, Gordon EA, Wickman K, Velimirovic B, Krapivinsky L, Clapham DE (1995) The G-protein-gated atrial K^+ channel I_{KACh} is a heteromultimer of two inwardly rectifying K^+-channel proteins. Nature 374:135–141
21. Kurachi Y, Nakajima T, Sugimoto T (1986) On the mechanism of activation of muscarinic K^+ channels by adenosine in isolated atrial cells: involvement of GTP-binding proteins. Pflugers Arch 407:264–274
22. Leaney JL, Dekker LV, Tinker A (2001) Regulation of a G protein-gated inwardly rectifying K^+ channel by a Ca^{2+}-independent protein kinase C. J Physiol 534:367–379
23. Mao J, Wang X, Chen F, Wang R, Rojas A, Shi Y, Piao H, Jiang C (2004) Molecular basis for the inhibition of G protein-coupled inward rectifier K^+ channels by protein kinase C. Proc Natl Acad Sci USA 101:1087–1092
24. Matsuura H, Sakaguchi M, Tsuruhara Y, Ehara T (1996) Activation of the muscarinic K^+ channel by P_2-purinoceptors via pertussis toxin-sensitive G proteins in guinea-pig atrial cells. J Physiol 490:659–671

25. Matsuura H, Ehara T (1996) Modulation of the muscarinic K^+ channel by P_2-purinoceptors in guinea-pig atrial myocytes. J Physiol 497:379–393
26. Matsuura H, Ehara T (1992) Activation of chloride current by purinergic stimulation in guinea pig heart cells. Circ Res 70:851–855
27. Matsuura H, Ehara T (1997) Selective enhancement of the slow component of delayed rectified K^+ current in guinea-pig atrial cells by external ATP. J Physiol 503:45–54
28. Matsuura H, Tsuruara Y, Sakaguchi M, Ehara T (1996) Enhancement of delayed rectifier K^+ current by P_2-purinoceptor stimulation in guinea-pig atrial. J Physiol 490:647–658
29. Meyer T, Wellner-Kienitz MC, Biewald A, Bender K, Eickel A, PottlT L (2001) Depletion of phosphatidylinositol 4,5-bisphosphate by activation of phospholipase C-coupled receptors causes slow inhibition but not desensitization of G protein-gated inward rectifier K^+ current in atrial myocytes. J Biol Chem 276:5650–5658
30. Musa H, Tellez JO, Chandler NJ, Greener ID, Maczewski M, Mackiewicz U, Beresewicz A, Molenaar P, Boyett MR, Dobrzynski H (2009) P2 purinergic receptor mRNA in rat and human sinoatrial node and other heart regions. Naunyn Schmiedebergs Arch Pharmacol 379:541–549
31. Neitzel KL, Hepler JR (2006) Cellular mechanisms that determine selective RGS protein regulation of G protein-coupled receptor signaling. Semin Cell Dev Biol 17:383–389
32. Nikolov EN, Ivanova-Nikolova TT (2004) Coordination of membrane excitability through a GIRK1 signaling complex in the atria. J Biol Chem 279:23630–23636
33. Parr CE, Sullivan DM, Paradiso AM, Lazarowski ER, Burch LH, Olsen JC, Erb L, Weisman GA, Boucher RC, Turner JT (1994) Cloning and expression of a human P_{2U} nucleotide receptor, a target for cystic fibrosis pharmacotherapy. Proc Natl Acad Sci USA 91:3275–3279
34. Pfaffinger PJ, Martin JM, Hunter DD, Nathanson NM, Hille B (1985) GTP-binding proteins couple cardiac muscarinic receptors to a K channel. Nature 317:536–538
35. Soejima M, Noma A (1984) Mode of regulation of the ACh-sensitive K-channel by the muscarinic receptor in rabbit atrial cells. Pflugers Arch 400:424–431
36. Stevens EB, Shah BS, Pinnock RD, Lee K (1999) Bombesin receptors inhibit G protein-coupled inwardly rectifying K^+ channels expressed in *Xenopus* oocytes through a protein kinase C-dependent pathway. Mol Pharmacol 55:1020–1027
37. Talasila A, Germack R, Dickenson JM (2009) Characterization of P2Y receptor subtypes functionally expressed on neonatal rat cardiac myofibroblasts. Br J Pharmacol 58:339–353
38. Thaning P, Bune LT, Hellsten Y, Pilegaard H, Saltin B, Rosenmeier JB (2010) Attenuated purinergic receptor function in patients with type 2 diabetes. Diabetes 59:182–189
39. Tsang S, Woo AY, Zhu W, Xiao RP (2010) Deregulation of RGS2 in cardiovascular diseases. Front Biosci (Schol Ed) 2:547–557
40. Vassort G (2001) Adenosine 5′-triphosphate: a P2-purinergic agonist in the myocardium. Physiol Rev 81:767–806
41. Von Kugelgen I (2006) Pharmacological profiles of cloned mammalian P2Y-receptor subtypes. Pharmacol Ther 110:415–432
42. Waldo GL, Harden TK (2004) Agonist binding and Gq-stimulating activities of the purified human $P2Y_1$ receptor. Mol Pharmacol 65:426–436
43. Wihlborg AK, Balogh J, Wang L, Borna C, Dou Y, Joshi BV, Lazarowski E, Jacobson KA, Arner A, Erlinge D (2006) Positive inotropic effects by uridine triphosphate (UTP) and uridine diphosphate (UDP) via $P2Y_2$ and $P2Y_6$ receptors on cardiomyocytes and release of UTP in man during myocardial infarction. Circ Res 98:970–976
44. Yasuda Y, Matsuura H, Ito M, Matsumoto T, Ding WG, Horie M (2005) Regulation of the muscarinic K^+ channel by extracellular ATP through membrane phosphatidylinositol 4,5-bisphosphate in guinea-pig atrial myocytes. Br J Pharmacol 145:156–165

A Connexin40 Mutation Associated With a Malignant Variant of Progressive Familial Heart Block Type I

Naomasa Makita, MD, PhD; Akiko Seki, MD, PhD; Naokata Sumitomo, MD, PhD; Halina Chkourko, MS; Shigetomo Fukuhara, PhD; Hiroshi Watanabe, MD, PhD; Wataru Shimizu, MD, PhD; Connie R. Bezzina, PhD; Can Hasdemir, MD; Hideo Mugishima, MD; Takeru Makiyama, MD, PhD; Alban Baruteau, MD; Estelle Baron, BS; Minoru Horie, MD, PhD; Nobuhisa Hagiwara, MD, PhD; Arthur A.M. Wilde, MD; Vincent Probst, MD, PhD; Hervé Le Marec, MD; Dan M. Roden, MD; Naoki Mochizuki, MD, PhD; Jean-Jacques Schott, PhD; Mario Delmar, MD, PhD

Background—Progressive familial heart block type I (PFHBI) is a hereditary arrhythmia characterized by progressive conduction disturbances in the His-Purkinje system. PFHBI has been linked to genes such as *SCN5A* that influence cardiac excitability but not to genes that influence cell-to-cell communication. Our goal was to explore whether nucleotide substitutions in genes coding for connexin proteins would associate with clinical cases of PFHBI and if so, to establish a genotype-cell phenotype correlation for that mutation.

Methods and Results—We screened 156 probands with PFHBI. In addition to 12 sodium channel mutations, we found a germ line *GJA5* (connexin40 [Cx40]) mutation (Q58L) in 1 family. Heterologous expression of Cx40-Q58L in connexin-deficient neuroblastoma cells resulted in marked reduction of junctional conductance (Cx40-wild type [WT], 22.2±1.7 nS, n=14; Cx40-Q58L, 0.56±0.34 nS, n=14; $P<0.001$) and diffuse localization of immunoreactive proteins in the vicinity of the plasma membrane without formation of gap junctions. Heteromeric cotransfection of Cx40-WT and Cx40-Q58L resulted in homogenous distribution of proteins in the plasma membrane rather than in membrane plaques in ≈50% of cells; well-defined gap junctions were observed in other cells. Junctional conductance values correlated with the distribution of gap junction plaques.

Conclusions—Mutation Cx40-Q58L impairs gap junction formation at cell-cell interfaces. This is the first demonstration of a germ line mutation in a connexin gene that associates with inherited ventricular arrhythmias and emphasizes the importance of Cx40 in normal propagation in the specialized conduction system. **(*Circ Arrhythm Electrophysiol.* 2012; 5:163-172.)**

Key Words: heart block ■ genes ■ ion channels ■ death sudden ■ gap junctions

Cardiac myocyte excitability in atria, His-Purkinje system, and ventricles is largely determined by the properties of voltage-gated sodium channels. Once activated, excitatory currents rapidly propagate to neighboring cells through low-resistance intercellular channels called gap junctions, which facilitate the synchronous contraction of the heart.[1,2] Loss of expression and function of cardiac gap junctions and sodium currents can severely impair action potential propagation, which sets the stage for life-threatening arrhythmias.[1,2] Although multiple mutations in genes coding for components of the voltage-gated sodium channel complex have been previously described in relation to arrhythmias and sudden death in young persons[3] and connexin40 (Cx40) mutations have been implicated in atrial fibrillation,[4,5] no study has identified an

Clinical Perspective on p 172

Received September 24, 2011; accepted January 9, 2012.

From the Department of Molecular Pathophysiology, Graduate School of Biomedical Sciences, Nagasaki University, Nagasaki, Japan (N. Makita); Cardiology, Tokyo Women's Medical University, Tokyo, Japan (A.S., N.H.); Pediatrics and Child Health, Nihon University School of Medicine, Tokyo, Japan (N.S., H.M.); Cardiology, New York University Medical School, New York, NY (H.C., M.D.); Cell Biology, National Cerebral and Cardiovascular Center Research Institute, Suita, Japan (S.F., N. Mochizuki); Cardiology, Niigata University Graduate School of Medical and Dental Sciences, Niigata, Japan (H.W.); Cardiology, National Cerebral and Cardiovascular Center, Suita, Japan (W.S.); Experimental Cardiology, Academic Medical Center, University of Amsterdam, Amsterdam, The Netherlands (C.R.B., A.A.M.W.); Cardiology, Ege University School of Medicine, Bornova, Izmir, Turkey (C.H.); Cardiovascular Medicine, Kyoto University Graduate School of Medicine, Kyoto, Japan (T.M.); l'institut du thorax, INSERM UMR915, Nantes, France (E.B., V.P., H.L., J.-J.S.); Cardiovascular Medicine, Shiga University of Medical Science, Otsu, Japan (M.H.); and Pharmacology and Medicine, Vanderbilt University, Nashville, TN (D.M.R.).

The online-only Data Supplement is available with this article at http://circep.ahajournals.org/lookup/suppl/doi:10.1161/CIRCEP.111.967604/-/DC1.

Correspondence to Naomasa Makita, MD, PhD, Department of Molecular Pathophysiology, Graduate School of Biomedical Sciences, Nagasaki University, 1-12-4 Sakamoto, 852-8523 Nagasaki, Japan. E-mail makitan@nagasaki-u.ac.jp

Circ Arrhythm Electrophysiol **is available at http://circep.ahajournals.org** **DOI: 10.1161/CIRCEP.111.967604**

association between germ line mutations in gap junction proteins and inherited ventricular arrhythmias in humans.

In this study, we investigated a group of patients with progressive familial heart block type I (PFHBI) (Online Mendelian Inheritance in Man 113900), also known as progressive cardiac conduction defect or Lenègre-Lev disease,[6,7] is a dominant inherited disorder of the His-Purkinje system. Affected individuals show electrocardiographic evidence of bundle branch disease (ie, right bundle branch block, left anterior or posterior hemiblock, complete heart block) with broad QRS complexes. The disease can progress from a normal ECG to right bundle branch block and from the latter to complete heart block. Affected individuals often present with family history of syncope, pacemaker implantation, and sudden death.[8] Although structural abnormalities have been invoked as a cause of the disease,[6,7] a number of patients present with normal cardiac structure and contractile function. Linkage analysis in a large South African PFHBI kindred[9] and a Lebanese kindred[10] mapped a causal locus on chromosome 19q13.3, and further work identified mutations in genes encoding for the transient receptor potential nonselective cation channel, subfamily M, member 4 (*TRPM4*) gene[11] at this locus. Haploinsufficiency of *SCN5A* and aging have been implicated in PFHBI,[8] and age-dependent manifestations of the disease have been recapitulated in mice.[12]

Here, we sought to expand on the association between PFHBI and mutations in genes relevant to action potential propagation; in particular, we assessed the possible association between nucleotide substitutions in connexin-coding genes and PFHBI. We evaluated 156 probands of diverse ethnic backgrounds from Asia, Europe, and North America given a clinical diagnosis of PFHBI. In addition to the sodium channel mutations previously reported,[13–15] we identified a germ line missense mutation in *GJA5* in a family with severe, early onset disease. This gene codes for the gap junction protein connexin40 (Cx40), which predominantly expresses in the atria and His-Purkinje system.[16] Heterologous expression experiments revealed that this novel mutation (Cx40-Q58L) significantly impaired the ability of Cx40 to form gap junction channels. Confocal microscopy showed that the Cx40-Q58L mutant but not the wild type (WT) failed to form plaques at sites of cell-cell apposition. Coexpression experiments indicated that the Cx40-WT protein provided only partial rescue of the Cx40-Q58L cellular phenotype. To our knowledge, this is the first description of a germ line mutation in a connexin gene associated with inherited ventricular arrhythmias. The results open the possibility of *GJA5* as a candidate gene for screening in patients with PFHB1, yet in the absence of further evidence, screening may be limited to the research environment rather than included as a part of the routine diagnostic examination.[17] The data also emphasize the importance of Cx40 in the maintenance of normal propagation in the specialized conduction system of the human heart.

Methods

Genetic Screening of PFHB1

Genomic screening by polymerase chain reaction and DNA sequencing was performed for *GJA5* (Cx40), *GJA1* (Cx43), *GJC1* (Cx45), *KCNQ1, KCNH2, SCN5A, KCNE1, KCNE2, KCNJ2, SCN1B, SCN4B, HCN4*. Primer information is provided in the online-only Data Supplement. All participating probands and family members gave written informed consent in accordance with standards (Declaration of Helsinki) and local ethics committees.

Plasmid Construction

A 1.1-kb Cx40-DNA fragment was subcloned into bicystronic plasmids pIRES2-EGFP and pIRES2-DsRED2. An EGFP or FLAG epitope was added at Cx40 C terminal to generate EGFP- or FLAG-tagged Cx40. Site-directed mutagenesis (Q58L) was performed with QuikChange. Primer information and additional details are provided in the online-only Data Supplement.

Cell Culture and Transfection

Constructs were introduced into connexin-deficient HeLa cells or mouse neuroblastoma (N2A) cells using Lipofectamine as per manufacturer's protocol.

Electrophysiology

Gap junction currents were recorded from transiently transfected N2A cell pairs using whole-cell double-patch clamp techniques as previously described.[18,19] Further details are provided in the online-only Data Supplement.

Immunocytochemistry and Western Blotting

HeLa cells, transfected with pEGFPN1-Cx40-WT, pCMV-FLAG-Cx40-Q58L, or both, were stained with anti-FLAG M2 antibody and Alexa546-labeled secondary antibody. EGFP and Alexa546 fluorescence images were recorded by confocal microscopy. For western blotting, N2A cells were transiently transfected with 3 μg of Cx40 plasmids. Two days after transfection, cells were lysed, and proteins were extracted and separated by conventional methods. Further details are provided in the online-only Data Supplement.

Statistical Analysis

Results are presented as mean±SEM. Mann-Whitney rank sum tests with Bonferroni post hoc correction were used in comparisons for which normality or equal variance assumptions were invalid. In other instances, differences between groups were assessed by 1-way ANOVA followed by Bonferroni post hoc correction. Statistical significance was assumed for $P<0.05$.

Results

Genetic Screening of PFHBI Probands

We genetically screened 156 probands given a clinical diagnosis of PFHBI. We identified 4 novel and 5 previously reported mutations in *SCN5A*,[13,15] 3 mutations in *SCN1B*,[14] and a novel germ line heterozygous missense mutation in exon 2 of the Cx40 gene *GJA5* (online-only Data Supplement Table I). Mutations were not found in connexin genes *GJA1* (Cx43) or *GJC1* (Cx45) or in the other genes screened (*KCNQ1, KCNH2, KCNE1, KCNE2, KCNJ2, HCN4,* or *SCN4B*). Of the novel *SCN5A* mutations, 1 caused a modification of the amplitude and voltage gating kinetics of the sodium current in heterologously expressing cells (online-only Data Supplement Figure I); 3 other mutant constructs failed to express functional channels, suggesting that patients carrying the mutation were functionally haploinsufficient for Nav1.5 (online-only Data Supplement Figure I). The *GJA5* mutation (c.173A>T) caused an amino acid substitution (glutamine [Q] replaced by leucine [L]) at position 58 in Cx40 (Cx40-Q58L) (Figure 1A and 1B). The mutation was absent in 400 alleles from unaffected control subjects and in the other 155 PFHBI probands. Screening of the entire gene

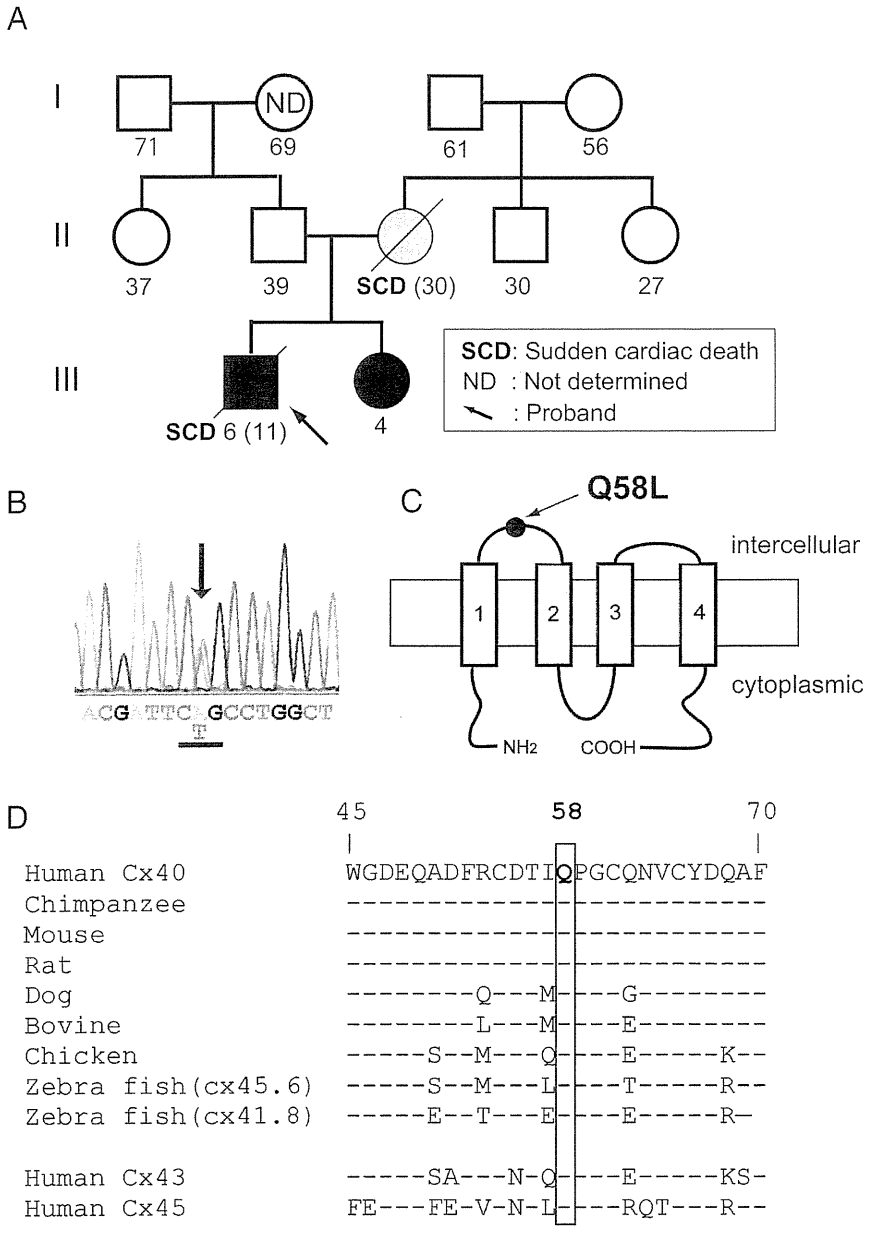

Figure 1. *GJA5* mutation identified in a family given the clinical diagnosis of progressive familial heart block type I. **A**, Family pedigree. Genetically affected and unaffected individuals are shown with closed and open symbols, respectively. The hatched circle indicates the proband's mother not genotyped; clinical data suggest that she was a de novo mutation carrier. Number below each symbol indicates the age at registration or age of SCD (parenthesis). **B**, Sequence electropherogram of exon 2 *GJA5* of proband. Arrow indicates heterozygous missense mutation of leucine (CTG) for glutamine-58 (CAG). **C**, Cx40 predicted membrane topology indicating position Q58 in first extracellular loop. **D**, Sequence alignment of human Cx40 and its homologues (residues 45–70). Notice the conservation in human Cx43 and Cx45. Dashes indicate residues identical with the top sequence. Cx indicates connexin.

panel (including *SCN5A* and *SCN1B*) revealed no other sequence modification in the DNA of this proband. Topological analysis placed amino acid 58 of Cx40 within the first extracellular loop (Figure 1C). The presence of glutamine in this position is highly conserved among *GJA5* orthologs, and 2 other cardiac connexins, Cx43 and Cx45 (Figure 1D). The clinical and genotypic characteristics of proband and tested family members are described next.

Clinical Phenotypes and Genotype of the PFHBI Pedigree With the *GJA5* Mutation

The proband, an 11-year-old boy at time of death, was first referred for evaluation when he was age 6 years because of ECG abnormalities. Although asymptomatic at that time, his ECG showed advanced atrioventricular block, complete left bundle branch block, and left axis deviation (Figure 2A). Echocardiography and cardiac scintigraphy did not reveal signs of structural heart disease. He experienced an episode of syncope at age 9; implantation of a permanent pacemaker was recommended by the physician but not authorized by the legal guardian. The proband died suddenly 2 years later during exercise (running), and the family declined postmortem examination. The proband's younger sister shares the Cx40-Q58L mutation. She is asymptomatic, with a QRS duration at the upper limit of normal, left axis deviation that has been progressive (online-only Data Supplement Table II), and QRS notch. These findings are consistent with impaired intraventricular conduction (Figure 2B). The mother died suddenly at age 30 after delivering the second child. An ECG on record, obtained when she was age 16, was similar to that of the proband (compare Figure 2C with 2A). In addition, a ventricular tachycardia was recorded during the recovery phase of an exercise stress test (online-only Data Supplement Figure II). DNA from the mother was not available for

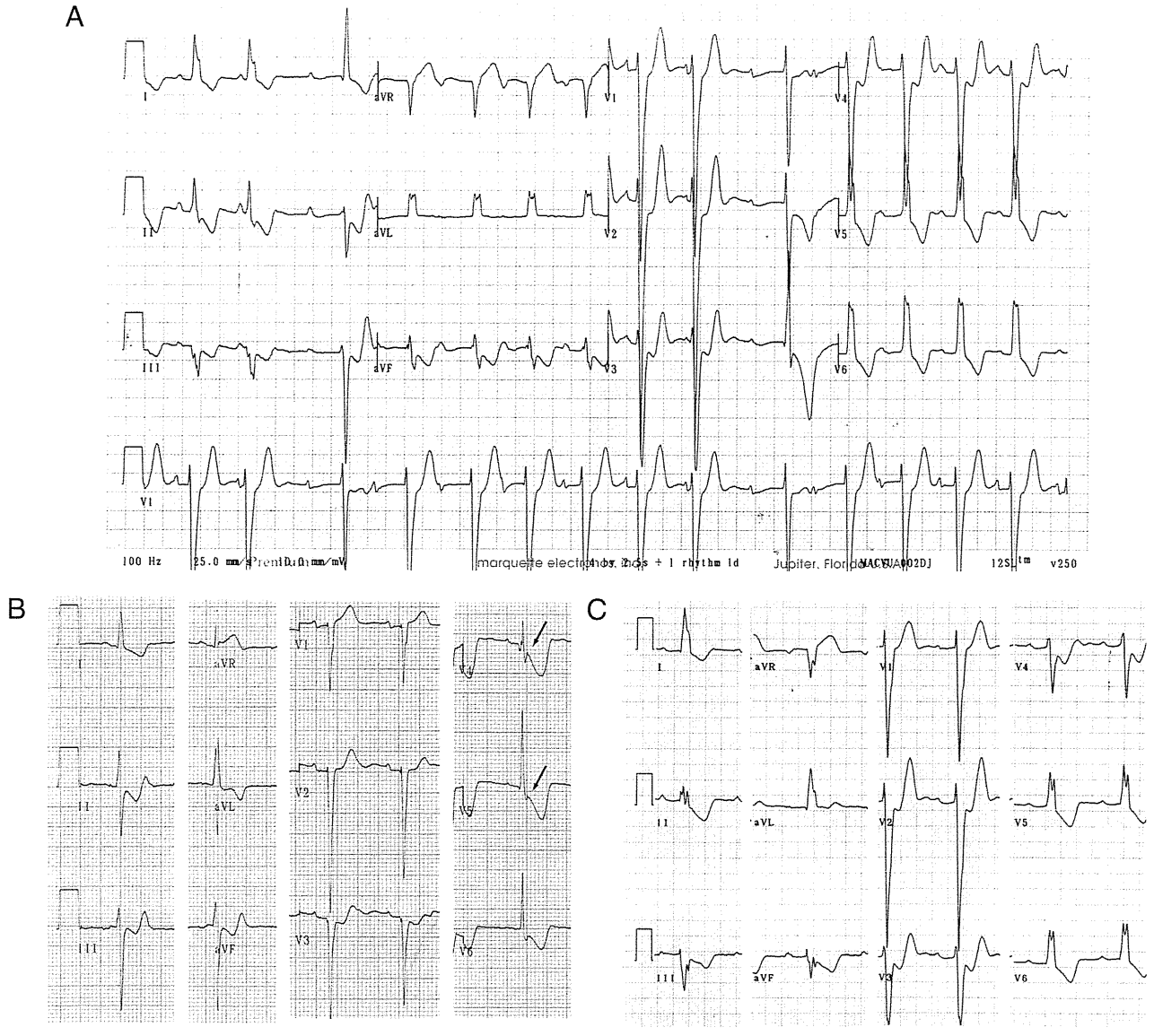

Figure 2. ECGs of proband and affected family members. **A**, ECG of proband at age 6 years, showing advanced atrioventricular block, complete left bundle branch block, and left axis deviation. Patient died suddenly 5 years later. **B**, ECG of proband's sister at age 6 years, showing QRS duration at the upper limit of normal, left axis deviation that has been progressive, and QRS notch in leads V4 and V5 (arrows) consistent with impaired intraventricular conduction. **C**, ECG of proband's mother at age 16 years, showing complete left bundle branch block and left axis deviation. She died suddenly at age 30.

examination. Other family members, including the proband's father, showed normal ECGs. DNA analysis of proband's father and maternal grandparents revealed absence of the Cx40-Q58L mutation. On the basis of clinical data and genotypic features of the proband and sister, it is most likely that the Cx40-Q58L mutation appeared de novo in the proband's mother. The data also indicate an early onset of PFHBI in this family compared with the natural history of the disease in most other cases.[8] As an initial step to assess the functional implications of the Cx40-Q58L mutation, modified constructs were transiently expressed in an exogenous system and evaluated for localization and function.

Electrophysiological Properties of Mutant Cx40-Q58L Channels

Connexin-deficient N2A cells were transiently transfected with cDNA for Cx40-WT or Cx40-Q58L; electrophysiological properties of homologous Cx40 channels were analyzed by conventional dual whole-cell patch clamp. Figure 3A shows representative junctional current traces elicited by a transjunctional voltage gradient of −60 mV. Average junctional conductance (Gj) decreased from 22.2±1.7 nS in cells expressing Cx40-WT (n=14) to 0.56±0.34 nS in cells expressing the Cx40-Q58L mutant (n=14; $P<0.001$). The probability of functional coupling, calculated by dividing the number of electrically coupled pairs by the number of pairs tested, was 100% and 57.1% for Cx40-WT and Cx40-Q58L, respectively.

Figure 3B depicts representative single-channel recordings elicited by a transjunctional voltage of −60 mV in cell pairs expressing Cx40-WT or Cx40-Q58L. Unitary events for WT channels displayed current transitions corresponding to 2 conducting states (O_1 and O_2) of 43.3 and 119.5 pS, respectively. Figure 3C shows the event histograms for both cell

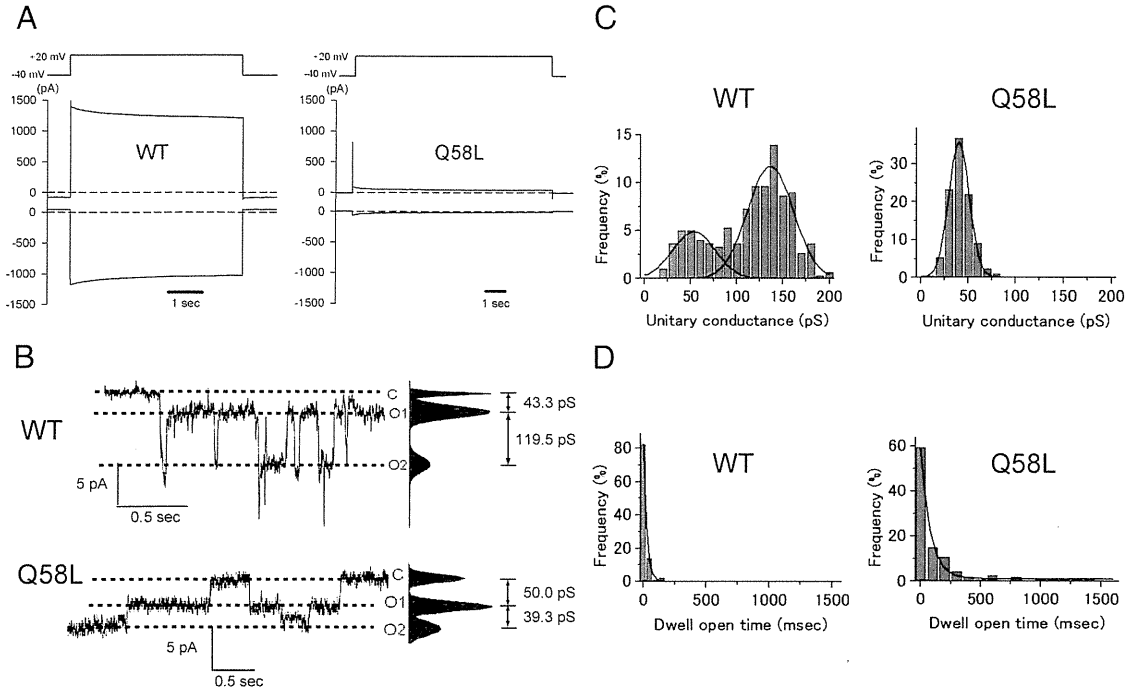

Figure 3. Whole-cell and single-channel properties of connexin40 (Cx40)-WT and Cx40–Q58L channels. **A**, Voltage pulse (top) and junctional current (bottom) from a homomeric WT cell pair (junctional conductance, 12.9 nS) and a Q58L cell pair (junctional conductance, 1.2 nS). **B**, Unitary currents recorded from homomeric Cx40-WT and Cx40–Q58L channels. O_1 and O_2 refer to 2 conducting (open) unitary levels of current. **C**, All-event histograms pooled from WT (n=3) and Q58L (n=3) cells with homologous channels. For WT, Gaussian peaks centered at 136.2±2.3 and 53.1±5.3 pS. For Q58L, best fit by a single Gaussian distribution centered at 40.2±0.3 pS (n=3). **D**, Frequency of events in relation to dwell open time. Binned data were fit by single exponentials (τ_{open} WT, 27.9±0.5 ms, 4 cells, 186 events; τ_{open} Q58L, 92.0±7.8 ms, 3 cells, 163 events). WT indicates wild type.

types (Cx40-WT, 3 cell pairs and 303 events; Cx40-Q58L, 3 cell pairs and 416 events). The histogram for the Cx40-WT channels was best described by 2 Gaussian distributions centered at 136.2±2.3 and 53.1±5.3 pS. In contrast, the histogram for Cx40-Q58L channels was best described by a single Gaussian function centered at 40.2±0.3 pS. Moreover, the length of time that a channel dwelled in the open state (dwell open time) was substantially longer for the Cx40-Q58L channels (92.0±7.8 ms, 3 cell pairs, 163 events) than for Cx40-WT channels (27.9±0.5 ms, 4 cell pairs, and 186 events) (Figure 3D). Of note, the Q58L mutation had a strong dominant effect on formation of heterotypic functional gap junctions. Cells were transfected with either pIRES2-EGFP-Cx40-WT or pIRES2-DsRED2-Cx40-Q58L, and heterotypic pairs were identified by fluorescence microscopy (an EGFP-expressing cell paired with a DsRED2-expressing cell). We recorded from 8 cell pairs and detected unitary current events in only 2 pairs. A total of 57 events were recorded, and average macroscopic junctional conductance was 0.04±0.03 nS. Collectively, the data demonstrated that the Q58L mutation significantly affects the biophysical properties of Cx40 channels and the overall ability of Cx40 gap junctions to form a low-resistance pathway between cells.

Electrophysiological Properties and Gap Junction Plaque Formation in Cells Coexpressing WT and Q58L Proteins

In the clinical cases identified, the Q58L mutation was detected in only 1 carrier allele. Therefore, we assessed the function of gap junctions in cells coexpressing WT and mutant proteins. N2A cells were cotransfected with cDNA for both GFP-tagged Cx40-WT and Cx40-Q58L (0.5 μg of pEGFPN1-Cx40-WT combined with 0.5 μg of pEGFPN1-Cx40-Q58L). Results were compared with those obtained when only 1 of the constructs (1 μg) was transfected. Cells expressing both constructs (WT/Q58L) showed intermediate conductance (15.4±3.7 nS, n=16) between WT (28.8±3.6 nS, n=16, $P<0.001$) and Q58L (0.28±0.11 nS, n=14, $P<0.001$) (Figure 4A). These values were comparable to those obtained using the bicistronic pIRES2-EGFP constructs (WT, 22.2±1.7 nS, n=14; WT/Q58L, 13.0±2.4 nS, n=17; Q58L, 0.56±0.34 nS, n=14). The coexpression results were consistent with those obtained using pIRES plasmids that tagged the cells both green and red, if cotransfected (online-only Data Supplement Figure I). The probability of finding functional coupling in cotransfected cells was 76.5%, which was intermediately between WT (100%) and Q58L (57.1%).

The characteristics of gap junction plaques observed in cells coexpressing WT and Q58L varied significantly between pairs (Figure 4B). Nearly one half of transfected (fluorescence-positive) cells exhibited clear and discrete gap junction plaques (arrow a), whereas the rest of fluorescent-positive cells showed a diffuse expression pattern and absence of well-defined plaques (arrow b). Fluorescence-positive and gap junction plaque-positive cells were counted in 10 different views for each group, and efficacy of gap junction plaque formation was statistically analyzed (Figure 4C) by calculating the ratio of cells with gap junction plaques

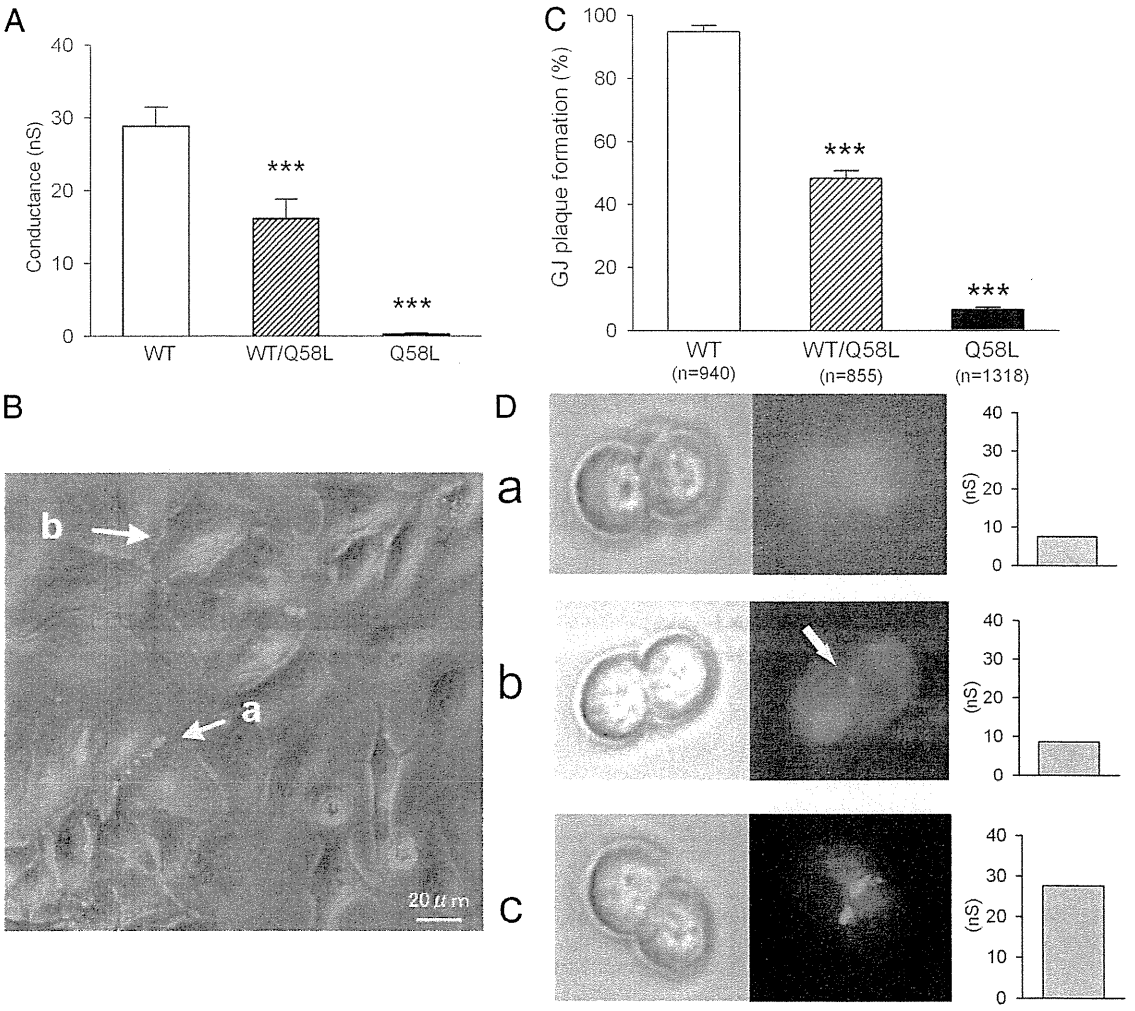

Figure 4. Macroscopic conductance and gap junction plaque morphology in cells coexpressing connexin40 (Cx40)-WT and Cx40-Q58L. **A**, Junctional conductance of cells transfected with plasmid pEGFPN1-Cx40-WT (1 μg), pEGFPN1-Cx40-Q58L (1 μg), or cotransfected with WT and Q58L (WT/Q58L, pEGFPN1-Cx40-WT 0.5μg+pEGFPN1-Cx40-Q58L 0.5 μg). **B**, Phase contrast/fluorescence overlay image of neuroblastoma cells transfected with WT/Q58L constructs. Arrow *a* points to gap junction plaque; arrow *b* points to an example of cells transfected but devoid of gap junction plaque. **C**, Efficacy of gap junction plaque formation was measured as the ratio between the number of gap junction plaque-positive cells and the number of fluorescent-positive cells (WT, n=940; WT/Q58L, n=855; Q58L, n=1318). **D**, Representative images of phase contrast (left), EGFP fluorescence (middle), and junctional conductance (right) from neuroblastoma cells cotransfected with pEGFPN1-Cx40-WT (0.25 μg) and pEGFPN1-Cx40-Q58L (0.25 μg). Three different examples illustrate the relation between plaque morphology and recorded junctional conductance. WT indicates wild type. ***$P<0.001$ compared with WT.

to the number of fluorescence-positive cells. In the Cx40-WT group, almost all fluorescent-positive cells exhibited clear gap junction plaques (94.9±1.9%, n=940), whereas there was a more-diffuse and homogenous pattern with only occasional plaque formation in the Cx40-Q58L group (6.6±0.7%, n=1318, $P<0.001$ compared with WT). In contrast, results varied widely in cells cotransfected with WT/Q58L; nearly one half of fluorescence-positive cells exhibited gap junction plaques similar to those observed in cells transfected with the WT construct (48.2±2.4%, n=855, $P<0.001$), whereas the rest showed a diffuse expression pattern similar to that of Cx40-Q58L. To establish a better correlation between plaque formation and junctional conductance, both variables were measured concurrently in the same cell pair for 39 N2A cell pairs where GFP-tagged plasmids of Cx40-WT and Cx40-Q58L were cotransfected. As shown in Figure 4D, about one half of GFP-positive cell pairs showed a very small Gj (<5 nS) and very few or negligible gap junction plaques (a). In the other half of cell pairs, small, dot-like junctional plaques correlated with intermediate Gj values (b), and there were clear, extensive gap junction plaques associated with Gj values >25 nS (c). Overall, we found significant heterogeneity in the extent of electric coupling, although the measurements of Gj correlated with the localization of proteins in transfected cells. These results indicate that the Q58L mutation significantly impairs the ability of cells to form gap junction plaques, although the effect is not purely dominant when both WT and mutant proteins are coexpressed.

Subcellular Distribution of WT and Q58L Cx40 in Transiently Transfected Cells

To further analyze the subcellular distribution of Cx40-WT and Cx40-Q58L proteins, the C terminal of Cx40-WT was

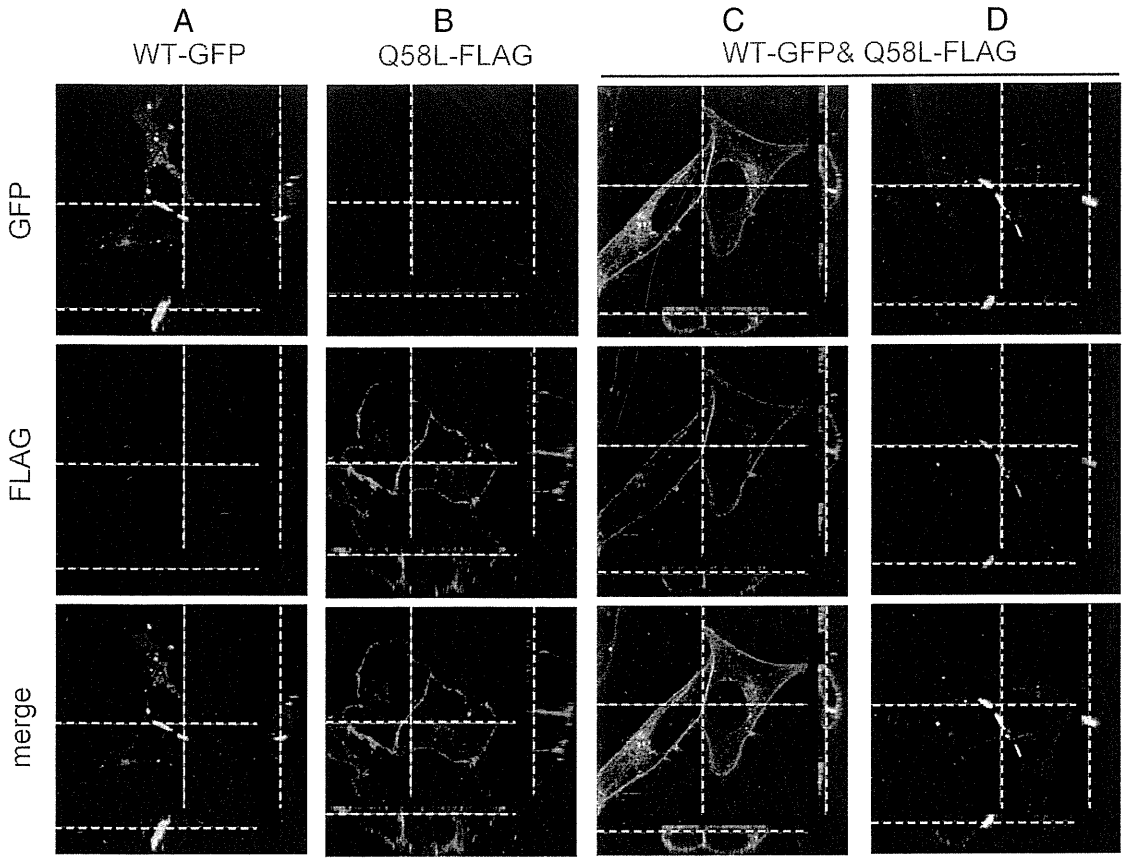

Figure 5. Subcellular distribution of connexin40 (Cx40)-WT and Cx40-Q58L in transiently transfected cells. HeLa cells were transiently transfected with pEGFPN1-Cx40-WT (3.0 μg) (**A**), pCMV-FLAG-Cx40-Q58L (3.0 μg) (**B**), or pEGFPN1-Cx40-WT (1.5 μg) plus pCMV-FLAG-Cx40-Q58L (1.5 μg) (**C**); immunostained for the respective tag protein; and visualized by confocal laser scanning microscopy. Notice that gap junction plaques (**A**) are absent in Q58L transfectants (**B**) and present in some (**D**) but not all (**C**) cotransfected cells. Bar=20 μm. WT indicates wild type.

tagged with GFP, whereas the C terminal of Cx40-Q58L was FLAG tagged. After transfection of N2A cells with the tagged constructs, the distribution of each protein was examined by confocal microscopy. As shown in Figure 5, green color indicates the position of GFP-tagged molecules, whereas red indicates the position of FLAG-tagged molecules. In cells transfected only with GFP-tagged Cx40-WT, fluorescence was consistently detected at sites of cell-cell apposition, following the pattern previously described for GFP-labeled gap junction plaques (Figure 5A). A similar distribution was found when cells were transfected with FLAG-tagged Cx40-WT (not shown). In contrast, most FLAG-tagged Cx40-Q58L signals were evenly distributed around the cell in the vicinity of the plasma membrane (Figure 5B). Biotinylation experiments showed that the Q58L mutation did not prevent the Cx40 protein from inserting into the membrane and presenting a domain-reachable form in the extracellular space (online-only Data Supplement Figure II). Micoscopy experiments in cells coexpressing GFP-tagged Cx40-WT and FLAG-tagged Cx40-Q58L proteins yielded results intermediate to those obtained when only 1 construct was expressed. Nearly one half of cell pairs showed that both proteins distributed homogenously at or near the cell membrane, without the formation of well-defined gap junction plaques (Figure 5C). These images resembled those obtained when only Cx40-Q58L proteins were expressed (Figure 5B, FLAG). In contrast, other cell pairs showed clustering of fluorescent signals within closely confined areas that appeared to be gap junction plaques (Figure 5D).

The experiments described herein led us to speculate that the distribution and function of heteromeric connexons is determined by their mutant subunit content, whereby formation (or not) of plaques and channels are determined, at least in part, by the abundance of expression of one protein over the other. As an initial step to probe this hypothesis, we took advantage of the characteristics of the bicistronic plasmid pIRES, in which the expression rate of the upstream gene is several-fold greater than that of the downstream gene,[20] and explored the functional properties of heteromeric connexons. Cx40-WT and GFP-tagged Cx40-Q58L were subcloned into the pIRES vector, either alone or in combination, in the specific orientations shown in Figure 6A. Protein expression levels of Cx40-WT and Cx40-Q58L were determined by immunochemistry. In contrast to the data obtained when Cx40-WT and GFP-tagged Cx40-Q58L plasmids were cotransfected at a 1:1 ratio (lane 6), expression of heteromeric pIRES plasmids WT-IRES-Q58L-EGFP (lane 3) and Q58L-EGFP-IRES-WT (lane 4) resulted in uneven protein expression levels of WT (40 kDa) and Q58L-EGFP (67 kDa), depending on their orientation in the pIRES vector. Based on

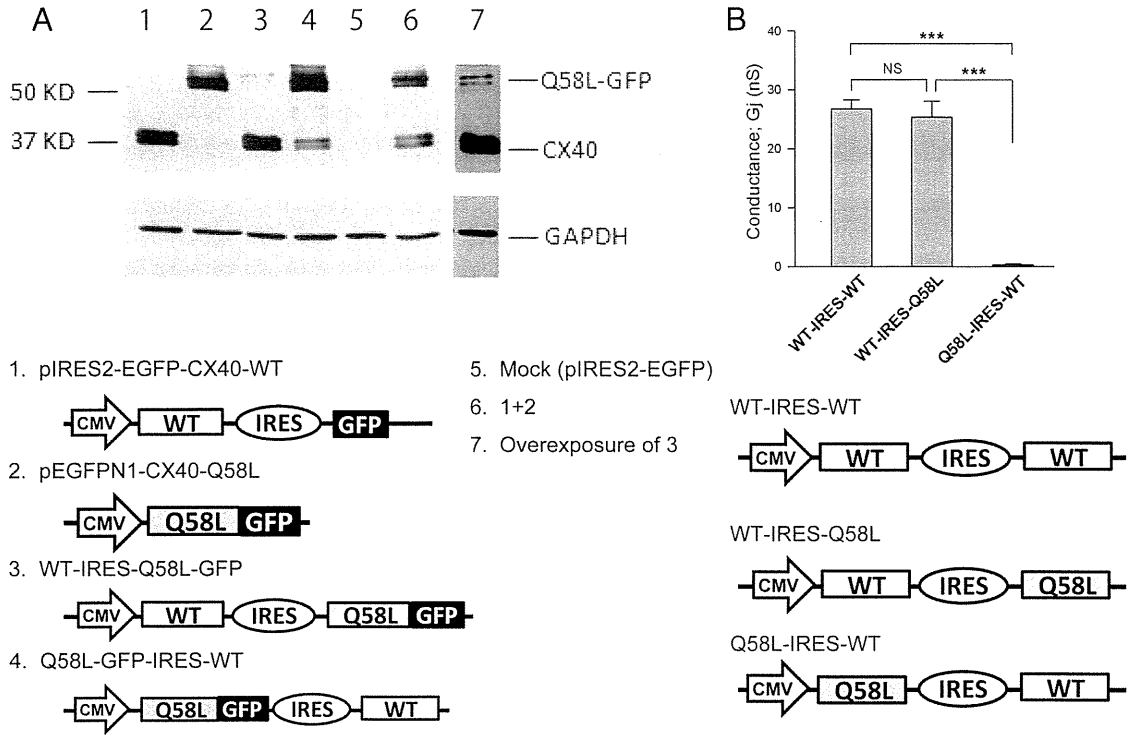

Figure 6. Mutant subunit abundance correlated with gap junction function. **A**, Neuroblastoma cells were transiently transfected with 3 μg Cx40 constructs in IRES plasmids. Cell lysates were analyzed by western blot using anti-Cx40 (top) and anti-GAPDH antibodies (bottom). The number in each lane corresponds to the plasmid noted below the image. Samples from cells cotransfected with plasmids 1 and 2 (1.5 μg each) were loaded on lane 6. Double bands of Cx40-WT (40 kDa) and Q58L-EGFP (67 kDa) are shown in lanes 3, 4, 6, and 7. Results were repeated in 3 separate experiments. Overexposure (lane 7) confirmed expression of the high-molecular-weight protein in lane 3. **B**, Junctional conductance of homomeric and heteromeric constructs (WT-IRES-Q58L and Q58L-IRES-WT). Conductance of cell pairs expressing WT-IRES-WT (n=17) was comparable to heteromeric construct WT-IRES-Q58L (n=17). However, converse heteromeric construct Q58L-IRES-WT (n=15) showed significantly reduced conductance ($P<0.001$ versus WT-IRES-WT and WT-IRES-Q58L). ***$P<0.001$. NS indicates not significant; WT, wild type.

these observations, we constructed a homomeric Cx40-WT plasmid (WT-IRES-WT) and heteromeric plasmids of Cx40-WT and Cx40-Q58L with different orientations (WT-IRES-Q58L and Q58L-IRES-WT) (Figure 6B). The junctional conductance of cell pairs expressing WT-IRES-Q58L (25.3±2.8 nS, n=17) was nearly indistinguishable from that of the homomeric plasmid WT-IRES-WT (27.8±1.4 nS, n=17, *P* not significant). By contrast, the converse heteromeric construct Q58L-IRES-WT showed substantially reduced junctional conductance (0.29±0.12 nS, n=15, $P<0.001$) comparable with that of the homomeric Q58L (0.56±0.34 nS) (Figure 3A). These results suggest that the final electrophysiological properties of the heteromeric connexons are determined predominantly by the numbers of mutant subunits in each gap junction rather than defined by a dominant-negative effect.

Discussion

Genetic screening confirmed the association of *SCN5A* and *SCN1B* with PFHB1[13–15] and revealed novel mutations within these genes (online-only Data Supplement Table I). More importantly, we identified a particularly severe, early onset case of PFHBI associated with a germ line mutation in *GJA5* in 2 blood relatives (proband and sister) given a clinical diagnosis of PFHBI. The data also indicate that the protein expressed (Cx40-Q58L) failed to form functional gap junctions in an exogenous expression system and decreased the probability of gap junction formation in cells coexpressing the WT protein.

So far, *SCN5A*, *SCB1B*, and *TRPM4* are the only genes associated with PFHB1.[11,13,14] The National Human Genome Research Institute database shows no association of *GJA5* single-nucleotide polymorphisms with arrhythmias or conduction system diseases. PR interval and QRS have been associated with several loci, including *SCN5A*, *SCN10A*, *NKX2.5*, and *TBX5*[21,22] but not *GJA5*, which is located at chromosome 1q21.1. Overall, the present results suggest that *GJA5* is a candidate gene associated with PFHBI, likely in a small fraction of the affected population. Yet, given the limited cosegregation observed in the reported family, we remain cautious in assigning a causative nature to the *GJA5* mutation. It will be of great interest to expand the screening of *GJA5* at the research level to identify other cases associated with amino acid changes in Cx40, although it may be premature to include *GJA5* as a part of the routine diagnostic screen.[17] The present results also emphasize the importance of Cx40 in the maintenance of normal cardiac rhythm.

To our knowledge, this is the first report of a germ line mutation in Cx40 associated with a high risk of ventricular arrhythmias (online-only Data Supplement Figure II). Other studies have shown somatic mutations of Cx40 or Cx43 in patients with idiopathic atrial fibrillation[5,23]; those mutations

were confined to the atria, and conduction abnormalities in the ventricles or His-Purkinje system were not observed. On the other hand, as in all cases involving identified genetic substrates for disease, the possibility of compound mutations in unexamined genes cannot be excluded. We do emphasize that the mutation led to a severe cellular phenotype in an exogenous expression system, supporting the argument that just the Q58L substitution can impair the formation of gap junctions necessary for propagation of action potentials between cells.

The results show that Cx40-Q58L was abundantly expressed in an exogenous system. The protein reached the vicinity of the cell membrane but failed to form gap junction plaques (Figure 5B). This result may be due to impaired docking of mutant hemichannels within the intercellular space because of the mutation in the extracellular loop (Figure 1C). During trafficking, connexin subunits oligomerize to form a hemichannel (or connexon). Once at the site of cell contact, connexons from apposing cells dock, sealing the hydrophilic path (the channel pore) from the extracellular space. The locking of 2 connexons into 1 gap junction channel is believed to stabilize connexin subunits in place, facilitating aggregation of other oligomers into their vicinity and eventually forming a plaque. Amino acid substitutions within the extracellular loop, as in Q58L, can prevent hemichannel docking and, thus, plaque formation.[24] The present biotinylation experiments indicate that the Q58L protein integrates into the cell membrane, supporting the notion that the inability of the Q58L mutation to form functional gap junctions is related to events that occur after the oligomer is delivered to the cell membrane and before a functional dodecamer converts into a functional channel in a gap junction plaque.

Results obtained in cells coexpressing both mutant and WT proteins clearly show that one subunit can significantly influence the fate of the other (Figure 5). This suggests that Cx40-Q58L subunits retain their ability to oligomerize not only with other mutant subunits, but also with the WT protein. The results also present an interesting paradigm in that neither the WT nor the mutant construct exerted a dominant effect over the other. After transfection with equal amounts of cDNA, we found cells where both WT and mutant proteins displayed the phenotype of the mutant construct, whereas in other cases, junctional plaques could be easily discerned (although an outline of the cell, likely resulting from the presence of the FLAG-tagged mutant protein, could still be observed [see red signal in Figure 5D]). These results can be explained if we assume that the probability of proper targeting and integration of a connexon into a plaque decreases as a function of the number of mutant subunits contained. For cotransfection, we used equal amounts of cDNA; however, it is very likely that each cell was transfected with variable amounts of each construct and, thus, expressed variable amounts of each protein. We speculate that a majority (though of unknown stoichiometry) of WT connexin subunits are required in a connexon for proper formation of functional gap junctions. Thus, if a cell captures an abundance of Q58L cDNA, most oligomers will contain an excess of mutant subunits, and gap junction formation will fail. If, on the other hand, that cell captures and expresses more of the WT cDNA, the distribution of the subunits within the oligomer will contain a majority of WT connexins, and the connexon will be properly integrated into a channel. This hypothesis will require further testing, although data presented in Figure 6 support the concept that success or failure of functional channel formation may relate to relative abundance of each protein (WT or mutant). If our hypothesis is correct, it suggests that the distribution of functional gap junctions in the His-Purkinje network of affected individuals could vary significantly among cells, depending on the extent of expression of each allele in each cell. The resulting phenotype may be that of a Purkinje network where gap junction-mediated coupling could be heterogeneous, setting the stage for local conduction block, microreentry, and ventricular arrhythmias at the Purkinje network or at the Purkinje-muscle junction.[1,2]

Overall, we show that both proband and sister have a genotype that (1) is absent in hundreds of control subjects and in the unaffected parent (the father), (2) disrupts an important functional domain of the protein, and (3) disrupts the formation of gap junction channels. The data therefore support the notion of an association between the Cx40 mutation and the clinical phenotype and emphasize the importance of future studies to assess the possible involvement of Cx40 mutations as causative of the disease.

Acknowledgments

We thank Dr A.L. George for critical reading of the manuscript and Mss M. Fukuoka and C.R. Ingram for technical assistance.

Sources of Funding

This work was supported by research grant 21590921 (to Dr Makita), Scientific Research B (to Dr Mochizuki), and Grant-in-Aid for Scientific Research on Innovative Areas (HD Physiology) 22136007 (to Dr Makita) from the Ministry of Education, Culture, Sports, Science and Technology, Japan; a Health and Labor Sciences Research Grant for research on measures for intractable diseases from the Ministry of Health (2010-145) (to Dr Makita); the Mitsubishi Pharma Research Foundation (to Dr Makita); the Japan-France Integrated Action Program (SAKURA) (to Drs Makita and Schott); The Naito Foundation (to Drs Makita and Seki); the Support Center for Women Health Care Professionals and Researchers 21590921 (to Dr Seki); and grants GM057691, HL106632 and HL087226 from the National Institutes of Health (to Dr Delmar).

Disclosures

None.

References

1. Saffitz JE, Lerner DL, Yamada KA. Gap junction distribution and regulation in the heart. In: Zipes DP, Jalife J, eds. *Cardiac Electrophysiology: From Cell to Bedside*. Philadelphia, PA: Saunders; 2004:181–191.
2. Park DS, Fishman GI. The cardiac conduction system. *Circulation*. 2011; 123:904–915.
3. Ruan Y, Liu N, Priori SG. Sodium channel mutations and arrhythmias. *Nat Rev Cardiol*. 2009:6:337–348.
4. Firouzi M, Ramanna H, Kok B, Jongsma HJ, Koeleman BPC, Doevendans PA, Groenewegen WA, Hauer RNW. Association of human connexin40 gene polymorphisms with atrial vulnerability as a risk factor for idiopathic atrial fibrillation. *Circ Res*. 2004;95:e29–e33.
5. Gollob MH, Jones DL, Krahn AD, Danis L, Gong X-Q, Shao Q, Liu X, Veinot JP, Tang ASL, Stewart AFR, Tesson F, Klein GJ, Yee R, Skanes AC, Guiraudon GM, Ebihara L, Bai D. Somatic mutations in the connexin 40 gene (*GJA5*) in atrial fibrillation. *N Engl J Med*. 2006;354:2677–2688.

6. Lenègre J. Etiology and pathology of bilateral bundle branch block in relation to complete heart block. *Prog Cardiovasc Dis.* 1964;6:409–444.
7. Lev M, Kinare SG, Pick A. The pathogenesis of atrioventricular block in coronary disease. *Circulation.* 1970;42:409–425.
8. Probst V, Kyndt F, Potet F, Trochu JN, Mialet G, Demolombe S, Schott JJ, Baro I, Escande D, Le Marec H. Haploinsufficiency in combination with aging causes SCN5A-linked hereditary Lenègre disease. *J Am Coll Cardiol.* 2003;41:643–652.
9. Brink PA, Ferreira A, Moolman JC, Weymar HW, van der Merwe P-L, Corfield VA. Gene for progressive familial heart block type I maps to chromosome 19q13. *Circulation.* 1995;91:1633–1640.
10. de Meeus A, Stephan E, Debrus S, Jean M-K, Loiselet J, Weissenbach J, Demaille J, Bouvagnet P. An isolated cardiac conduction disease maps to chromosome 19q. *Circ Res.* 1995;77:735–740.
11. Kruse M, Schulze-Bahr E, Corfield V, Beckmann A, Stallmeyer B, Kurtbay G, Ohmert I, Schulze-Bahr E, Brink P, Pongs O. Impaired endocytosis of the ion channel TRPM4 is associated with human progressive familial heart block type I. *J Clin Invest.* 2009;119:2737–2744.
12. Royer A, van Veen TAB, Le Bouter S, Marionneau C, Griol-Charhbili V, Leoni A-L, Steenman M, van Rijen HVM, Demolombe S, Goddard CA, Richer C, Escoubet B, Jarry-Guichard T, Colledge WH, Gros D, de Bakker JMT, Grace AA, Escande D, Charpentier F. Mouse model of SCN5A-linked hereditary Lenègre's disease. Age-related conduction slowing and myocardial fibrosis. *Circulation.* 2005;111:1738–1746.
13. Schott JJ, Alshinawi C, Kyndt F, Probst V, Hoorntje TM, Hulsbeek M, Wilde AA, Escande D, Mannens MM, Le Marec H. Cardiac conduction defects associate with mutations in SCN5A. *Nat Genet.* 1999;23:20–21.
14. Watanabe H, Koopmann TT, Le Scouarnec S, Yang T, Ingram CR, Schott JJ, Demolombe S, Probst V, Anselme F, Escande D, Wiesfeld AC, Pfeufer A, Kaab S, Wichmann HE, Hasdemir C, Aizawa Y, Wilde AA, Roden DM, Bezzina CR. Sodium channel beta1 subunit mutations associated with Brugada syndrome and cardiac conduction disease in humans. *J Clin Invest.* 2008;118:2260–2268.
15. McNair WP, Ku L, Taylor MRG, Fain PR, Dao D, Wolfel E, Mestroni L; Familial Cardiomyopathy Registry Research Group. SCN5A mutation associated with dilated cardiomyopathy, conduction disorder, and arrhythmia. *Circulation.* 2004;110:2163–2167.
16. Miquerol L, Meysen S, Mangoni M, Bois P, van Rijen HVM, Abran P, Jongsma H, Nargeot J, Gros D. Architectural and functional asymmetry of the His-Purkinje system of the murine heart. *Cardiovasc Res.* 2004;63:77–86.
17. Ackerman MJ, Priori SG, Willems S, Berul C, Brugada R, Calkins H, Camm AJ, Ellinor PT, Gollob M, Hamilton R, Hershberger RE, Judge DP, Le Marec H, McKenna WJ, Schulze-Bahr E, Semsarian C, Towbin JA, Watkins H, Wilde A, Wolpert C, Zipes DP. HRS/EHRA expert consensus statement on the state of genetic testing for the channelopathies and cardiomyopathies. *Heart Rhythm.* 2011;8:1308–1339.
18. Seki A, Coombs W, Taffet SM, Delmar M. Loss of electrical communication, but not plaque formation, after mutations in the cytoplasmic loop of connexin43. *Heart Rhythm.* 2004;1:227–233.
19. Anumonwo JMB, Taffet SM, Gu H, Chanson M, Moreno AP, Delmar M. The carboxyl terminal domain regulates the unitary conductance and voltage dependence of connexin40 gap junction channels. *Circ Res.* 2001;88:666–673.
20. Bochkov YA, Palmenberg AC. Translational efficiency of EMCV IRES in bicistronic vectors is dependent upon IRES sequence and gene location. *Biotechniques.* 2006;41:283–284.
21. Holm H, Gudbjartsson DF, Arnar DO, Thorleifsson G, Thorgeirsson G, Stefansdottir H, Gudjonsson SA, Jonasdottir A, Mathiesen EB, Njolstad I, Nyrnes A, Wilsgaard T, Hald EM, Hveem K, Stoltenberg C, Lochen M-L, Kong A, Thorsteinsdottir U, Stefansson K. Several common variants modulate heart rate, PR interval and QRS duration. *Nat Genet.* 2010;42:117–122.
22. Pfeufer A, van Noord C, Marciante KD, Arking DE, Larson MG, Smith AV, Tarasov KV, Muller M, Sotoodehnia N, Sinner MF, Verwoert GC, Li M, Kao WHL, Kottgen A, Coresh J, Bis JC, Psaty BM, Rice K, Rotter JI, Rivadeneira F, Hofman A, Kors JA, Stricker BHC, Uitterlinden AG, van Duijn CM, Beckmann BM, Sauter W, Gieger C, Lubitz SA, Newton-Cheh C, Wang TJ, Magnani JW, Schnabel RB, Chung MK, Barnard J, Smith JD, Van Wagoner DR, Vasan RS, Aspelund T, Eiriksdottir G, Harris TB, Launer LJ, Najjar SS, Lakatta E, Schlessinger D, Uda M, Abecasis GR, Muller-Myhsok B, Ehret GB, Boerwinkle E, Chakravarti A, Soliman EZ, Lunetta KL, Perz S, Wichmann HE, Meitinger T, Levy D, Gudnason V, Ellinor PT, Sanna S, Kaab S, Witteman JCM, Alonso A, Benjamin EJ, Heckbert SR. Genome-wide association study of PR interval. *Nat Genet.* 2010;42:153–159.
23. Thibodeau IL, Xu J, Li Q, Liu G, Lam K, Veinot JP, Birnie DH, Jones DL, Krahn AD, Lemery R, Nicholson BJ, Gollob MH. Paradigm of genetic mosaicism and lone atrial fibrillation: physiological characterization of a connexin 43-deletion mutant identified from atrial tissue. *Circulation.* 2010;122:236–244.
24. Sosinsky GE, Nicholson BJ. Structural organization of gap junction channels. *Biochim Biophys Acta.* 2005;1711:99–125.

CLINICAL PERSPECTIVE

Progressive familial heart block type I, also known as progressive cardiac conduction defect, is an inherited form of cardiac conduction system dysfunction that can lead to severe heart rhythm disturbances, including sudden cardiac death. The genetic causes of this disease are poorly understood. Here, we genetically screened 156 patients with progressive familial heart block type I. In addition to mutations in genes of the voltage-gated cardiac sodium channel complex (*SCN5A* and *SCN1B*), we found a novel germ line mutation in *GJA5,* the gene encoding the gap junction protein connexin40. The disease had an early onset and was associated with otherwise unexplained sudden cardiac death in the proband and his mother. The proband's sister is also affected. Cellular phenotype analysis revealed impaired gap junction formation at cell-cell interfaces and marked reduction of junctional conductance in cells expressing the mutated connexin40 protein. The results emphasize the importance of connexin40 in normal electrical propagation in the cardiac conduction system and open the possibility of including *GJA5* as a target gene for study in patients with progressive familial heart block type I.

SUPPLEMENTAL MATERIAL

SUPPLEMENTAL METHODS

1. Genetic screening of PFHB1

The exon 2 of *GJA5* and exon 3 of *GJC1* that cover the entire coding region of the Cx40 and Cx45, respectively, were amplified by PCR from genome DNA using following primer sets.

GJA5	Forward (Cx40-F2)	5'-TGGAATCCCAGAACATGATAGA-3'
	Reverse (Cx40-R2)	5'-TCAGTTCAGAAGGGACACGTCT-3'
GJC1	Forward (Cx45-F1)	5'-GAGCCACCCTACCCAACTGA-3'
	Reverse (Cx45-R1)	5'-ACCAGAGCCAAATGTTTACTCAA -3'

The coding regions of *KCNQ1*, *KCNH2*, *SCN5A*, *KCNE1*, *KCNE2*, *KCNJ2*, *SCN1B*, *SCN4B*, *HCN4*, *GJA1* (Cx43) were amplified by PCR using exon flanking intronic primers as previously described.[1-8] Direct DNA sequencing was performed using ABI 3130 genetic analyzer (Applied Biosystems).

2. Plasmid construction

A 1.1-kilobase DNA fragment, encompassing the entire coding region of Cx40, was amplified by PCR from human genomic DNA using the following primers.

Forward (Cx40-F7)	5'-GAAGATCTCACCATGGGCGATTGGAGC TTCCT-3'
Reverse (Cx40-R2X)	5'-GGAATTCACACTGATAGGTCATCTG-3'

(Underlines represent the restriction recognition sequences for BglII and EcoRI, respectively) The PCR fragment was digested with BglII/EcoRI and subcloned into a bicystronic plasmid pIRES2-EGFP or pIRES2-DsRED2 (Takara Bio), for visual identification of cells expressing